SYNTHESIS AND SIZE DEPENDENT PROPERTIES OF MULTIFERROIC $BiFeO_3$ NANOPARTICLES.

BY

Mehedi Hasan Rizvi

STUDENT NUMBER 0413172005 p

THIS THESIS PAPER IS SUBMITTED TO THE DEPARTMENT OF GLASS AND CERAMIC ENGINEERING IN PARTIAL FULFILLMENT OF THE REQUIREMENTS FOR THE DEGREE OF MASTER OF SCIENCE IN GLASS AND CERAMIC ENGINEERING

DEPARTMENT OF GLASS AND CERAMIC ENGINEERING
BANGLADESH UNIVERSITY OF ENGINEERING AND TECHNOLOGY

CANDIDATES’ DECLARATION

IT IS HEREBY DECLARED THAT THIS THESIS PAPER OR ANY PART OF IT HAS NOT BEEN SUBMITTED ANYWHERE ELSE FOR THE AWARD OF ANY DEGREE

…………………………………………

Mehedi Hasan Rizvi
M.Sc. Engg., GCE, BUET

The thesis titled “Synthesis and size dependent properties of multiferroic $BiFeO_3$ nanoparticles” submitted by Mehedi Hasan Rizvi, student no 0413172005 P, session April 2013 has been accepted as satisfactory in partial fulfillment of the requirements for the degree of Master of Science in Glass and Ceramic Engineering on April 28, 2015.

Board of Examiners

. . . .

Chairman
Dr. Md. Fakhrul Islam
Professor & Head, Department of Glass & Ceramic Engineering, BUET, Dhaka, 1000.

. . . .

Member
Dr. M. A. Matin
Assistant Professor, Department of Glass & Ceramic Engineering, BUET, Dhaka, 1000.

. . . .

Member
Dr. Mohammed Abdul Basith
Assistant Professor, Department of Physics, BUET, Dhaka, 1000.

. . . .

Member (External)
Dr. Golam Mohammed Bhuiyan
Professor, Department of Theoretical Physics, University of Dhaka, Dhaka.

DEDICATION

To almighty Allah,

My beloved parents

And

Teachers

ACKNOWLEDGEMENTS

In the name of Allah, the Most Gracious and the Most Merciful

Alhamdulillah, all praises to almighty Allah for the strengths and His blessing in completing this thesis.

I would like to express my sincere gratitude to my thesis supervisor **prof. Md. Fakhrul Islam** for his constant motivation and support during the course of my work in the last two years. I truly appreciate and value his esteemed guidance and encouragement from the beginning to the end of this thesis. I am indebted to him for having helped me shape the problem and providing insights towards the solution.

I am immensely grateful to **Dr. A. K. M. Hakim** for his interest in my work, and encouragement and insight through these years. It was his guidance and support that helped me through all the difficult time. I will surely benefit from his creative thoughts, suggestions and dedication throughout the rest of my life. The same gratitude goes to **Dr. M. A. Matin** for his kind help and support on my research and my life during the past two years.

A special word of thanks to the members of the multiferroic group: **Rubayyat Mahbub, Arman Hussain, Takian Fakhrul** for their thoughtful discussions as well as sharing a great time with me in this group. *This project would not have gone so well without their contribution at the* forefront of this research.

I specially thank the Department of Glass and Ceramic Engineering (GCE), BUET and all of its members. Without their constant assistance this work would not have been possible. Without the lab facilities and raw materials provided by GCE my research project would have remained undone.

I convey my heartiest regards to **Dr. Md. *Nazrul Islam Khan***, Senior Scientific Officer, Materials Science Division, AEC, Dhaka, for their support with the XRD. I also express my sincere gratitude to **Md. Sarowar Hossain**, PhD student, S. N. Bose National Centre for Basic Sciences for his support with the VSM measurement.

Above all, I would like to thank all my family members and friends whose direct and indirect support helped me completing my project in time. This thesis would have been impossible without their perpetual moral support.

ABSTRACT

Utilization of Bismuth Ferrite ($BiFeO_3$) into modern device applications is restricted by its very low magnetic moments and high leakage current. Enhancement in magnetization is a real challenge for multiferroic $BiFeO_3$ in the context of device miniaturization and high density information storage system. In this study a significant improvement in magnetization has been recorded for $BiFeO_3$ nanoparticles, exploiting the beneficial effect of size confinement and low shape anisotropy. $BiFeO_3$ nanoparticles with different size in the range of 21-68 nm are synthesized via modified Pechini sol-gel approach. Ethylene glycol with a concentration of 0.05M has been successfully used as surfactant agent during synthesis process. An effective organic acid (acetic acid) is used for washing purpose instead of conventional use of nitric acid. X-ray diffraction result confirms pure, well crystallized and isotrophic regular shaped $BiFeO_3$ annealed at temperature lower than 600°C, compared to more than 800°C for the traditional solid-state sintering process. A strong size-dependent magnetization which increases with decreasing particle size is confirmed with a value of 1.4 emu/g for 40 nm particles in contrast to 7.5 emu/g for 21 nm particles. The homogeneous shape and distribution of the synthesized particles is found to be associated with the improved ferromagnetic properties.

Table of Contents

List of Figures

List of Tables

CHAPTER 1

INTRODUCTION

1.1 Background of the research:

Understanding the electric and magnetic properties of solid and especially crystalline materials has been the driving force of condensed matter physics, both for modern technological applications and for fundamental physics investigation. One technological application concerns data storage. In order to encode binary bits, materials used for memories need to have two nonvolatile and rewritable states. Ferroic materials, in particular ferromagnetic and ferroelectric materials, have proven particularly useful in current memorie devices.

Similarly ferromagnetic materials exhibit two stable and opposite states of spontaneous magnetization that can be reversed by a suitable magnetic field. Regions of uniform magnetization known as domains can therefore be used to encode binary bits. In the past decade, advances in atomic and nanoscale growth and characterization techniques have led to the study and exploitation of a range of new magnetic phenomena related to the spin of electrons in addition to their well known charge properties. Examples include colossal and giant magnetoresistive materials, in which magnetic fields cause order of magnitude changes in conductivity. Some technological applications such as sensors, read-heads and memories based on giant magnetoresistive materials are already commercially available, while many other proposed technologies, such as spin valves and spin transistors, are still under development.

Ferroelectric materials exhibit two stable and opposite states of spontaneous electrical polarization that can be switched by a suitable electric field. In parallel with ferromagnetic materials, they are useful for memory applications. Ferroelectrics are also pyroelectric, which means that their dipolar moment is temperature dependent, and piezoelectric, responding with an electric potential to applied mechanical stress and vice versa. In addition to ferroelectric random access memories (FeRAM), ferroelectrics are therefore used in a range of technological applications, including transducers, actuators and capacitors (because of their high dielectric permittivity).

Especially interesting for technological applications as well as fundamental research are materials in which both types of behavior can be combined. Materials that are simultaneously ferroelectric and ferromagnetic belong to a class known as multiferroic materials, and have all the potential for use in technological applications of both their parent materials. Moreover, since the coexistence of these two orders could potentially allow their cross-coupling through the magnetoelectric effect, an extra level of complexity in their fundamental physics and a whole range of new functionalities can be envisaged. Applications include multiple-state memory elements, in which data can be stored both ferromagnetically and ferroelectrically, and novel memory media, which could allow ferroelectric data writing to be combined with ferromagnetic reading [1].

However, there is a dearth of materials exhibiting multiferroic behavior in a single phase. Theoretical studies have shown that the usual atomic-level mechanisms for ferromagnetism and ferroelectricity are quite different. Ferroelectricity requires B-site ions with d^0 electrons, whereas the magnetism requires partially filled d^j electrons [2]. The perovskite $BiFeO_3$ is one of the few known magnetoelectric multiferroics that shows both ferroelectric and ferromagnetic behavior in a single phase. It has high phase transition temperatures (i.e. Curie temperature ~830 °C and Neel temperature ~370 °C) [3]. Because of its high transition temperatures, $BiFeO_3$ is considered as highly promising multiferroic material for practical applications.

The crystal structure of $BiFeO_3$ is described as rhombohedrally distorted perovskite with the space group R3c [4-6]. High resolution neutron diffraction studies have shown that the magnetic order of BFO is antiferromagnetic with G-type spin configuration. The combined action of exchange and spin-orbit interactions causes spin canting away from the perfect antiferromagnetic ordering resulting in a helical antiferromagnetic spin structure with a period of ~62 nm [7-10]. The helimagnetic structure results superimposed spiral spin arrangement canceling out macroscopic magnetization in bulk. Like many other materials, $BiFeO_3$ also shows peculiar behavior with decreasing particle size below a critical value. The $BiFeO_3$ nanoparticles show significant ferromagnetic order at room temperature which is quite different from the antiferromagnetic M–H relationship in bulk $BiFeO_3$. Previous reports claimed that a structural anomaly arises for the nanoparticles with size close to the 62 nm which is the basis for manifestation of ferromagnetism in this unique structure with uncompensated spiral spin modulation [10-12].

Generally, conventional solid state reaction and/or rapid liquid phase sintering of Bi_2O_3 and Fe_2O_3 are adopted to prepare bulk $BiFeO_3$ ceramic materials. Recently, wet chemical methods have received great attention for the synthesis of $BiFeO_3$ materials [13]. In this work a detail synthesis procedure to obtain pure $BiFeO_3$ powders and their structural and magnetic characterization have been outlined.

1.2 Recent trends of research on oxides:

Since very beginning metal oxides have been the most focused study from application as well as fundamental physics point of view. Their properties are strongly related to their structure, and variety of interesting physics has been witnessed on varying the external stimuli such as temperature and pressure. These properties have not only opened the door for various applications but also a better understanding of the physics involved. Some of the interesting properties include superconductivity, ferroelectricity, magnetism and multiferroicity.

1.2.1 Superconducting Oxides:

Until Bednorz & Muller reported superconductivity (1986) at ~23K in an oxide based compound, the superconducting phenomenon was considered only as low (Helium) temperature business and hence limited applications. Soon other oxide based superconductors were discovered whose superconducting transition temperature was much above that predicted by BCS theory for conventional superconductors, hence termed high temperature superconductor (HTS). Some of the HTS are listed in the chronological order of transition temperature in table-1.1 [14].

Table 1.1: List of some important high temperature superconducting materials

Material	T_c (K)
$YBa_2Cu_3O_7$ (YBCO)	90
$Bi_2Sr_2Ca_{1-x}Cu_nO_{2n+4}$ (BSSCCO)	122
$TiBa_2Ca_{n-1}Cu_nO_{2n+4}$(TBSSCO)	127

$TiBa_2Ca_{n-1}Cu_nO_{2n+3}$(TBSSCO)	122
$HgBa_2Ca_{n-1}Cu_nO_{2n+2}$	128

1.2.2 Ferroelectic Oxides:

Ceramic oxides with non-centrosymmentric perovskite structure generally show ferroelectricity. These oxides are used in bulk and thin film form for various applications. The ferroelectric properties of these oxides make them for use as non-volatile memory. The piezoelectric property of these materials enhances their use in actuators and ultrasound imaging. The high dielectric constant of these materials facilitates there use in capacitors and memory devices. The ferroelectric, piezoelectric and dielectric properties of the material are enhanced by doping the material with suitable dopants [15]. Now the current trend is to synthesize the ferroelectric oxides which give above properties at room temperature, for their applications. These oxides include $BaTiO_3$, $CaTiO_3$, $PbTiO_3$ and $SrTiO_3$ along with suitable dopants. Due to toxicity and high volatility of Lead (Pb), now a day there is awareness for synthesizing the lead free ceramic oxides for ferroelectric application. The different ferrolelectic oxides with their dielectric constant values are given in table 1.2.

Table 1.2: List of some ferroelectric materials

Materials	Dielectric constant
$SrTiO_3$	310
$Ba_{1-x}Sr_xTiO_3$	500
$BaTiO_3$	1250–10,000 (20–120 °C)
$CaTiO_3$	300
$(La,Nb,Zr,Ti)PbO_3$	500–6000

1.2.3 Magnetic Oxides:

Magnetic materials have become an integral part of our day-to-day life, owing to their various applications in different areas. Generally magnetic materials can be classified in soft and hard form, from the view point of magnetic property. The soft magnets are the magnets having low coercivity in the hysteresis loop and vice versa. The magnetic oxides are generally soft magnets. Due to low coercivity they are used into an alternating magnetic field [15]. They show excellent magnetic property in high frequency as compared with metal magnetic materials. They show high electrical resistivity and smaller eddy current loss. These soft magnetic oxides generally include ferrites, magnetites and cobaltites. Generally soft ferrites exist in two types of structures, i.e., spinel type and garnate type. They show the properties like high Curie temperature, high permeability and high stability. Transition metals like iron (Fe), cobalt (Co) manganese (Mn) and nickel (Ni) combining with oxygen and other materials results various oxides [15]. Various magnetic oxides with their magnetic flux density and Curie temperature values are listed in the table 1.3.

Table 1.3: List of some magnetic materials with their corresponding Curie temperatures.

Chemical formula	Magnetic flux density (Tesla) at room temperature	Ferromagnetic Curie temperature(T_c) in K
$MnFe_2O_4$	400	570
$CoFe_2O_4$	480	790
$NiFe_2O_4$	270	860
Y_3FeO_{12}	135	550
$Ba_3Co_2Fe_{24}O_{41}$	270	683

1.2.4 Multiferroic Oxides:

These oxides have the unique properties of both ferromagnetism and ferroelectricity in a single crystal. This opens broader applications in transducers, magnetic field sensors and information storage industry. These include $BiFeO_3$, $BiMnO_3$, $TbMnO_3$, $TbMn_2O_5$, $YMnO_3$ and $LuFeO_4$. Among these oxides $BiFeO_3$ (**BFO**) is the only material which gives ferroelectricity and antiferromagnetism at room temperature [1].

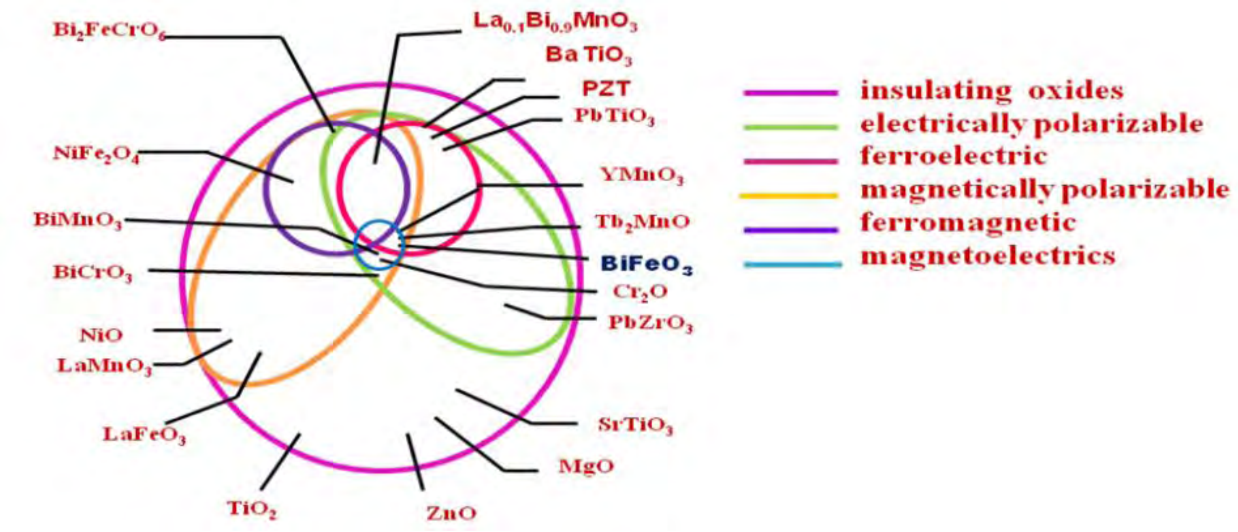

Figure 1.1: Representation of various oxides categorized by their behavior in electric and magnetic field.

Due to coexistence of both ferromagnetism and ferroelectricity in the same material, it is expected to exhibit ferromagnetic & ferroelectric properties or a coupling of these two properties in a single material. This increases the current range of application and moreover interesting physics may be observed. Presently lot of research work is carried out on this particular field in different forms like bulk, powder, thin film and nanostructure.

1.3 Motivation of the research:

One of the most challenging directions in condensed matter research is correlated to oxide structures. Such systems possess interacting charge, spin, orbital and lattice degrees of freedom and they often form novel electronic and magnetic phases. Fortunately, we can control these phases through stress, electric and magnetic fields, giving great potential for applications in fields such as information storage and communications. Multiferroic materials (for instance BFO) are currently attracting a great deal of attention. As BFO is a room temperature multiferroic, it is an obvious candidate for applications.

Ferroelectric random access memories (FeRAMs) have recently achieved faster access speeds (5 ns), higher densities (256 Mb) and embodiments in several traditional materials (Pb(Zr,Ti)O_3, (Ba,Sr)TiO3), but they are limited by the need for a destructive read and reset operation and suffer from atmospheric contamination. The modified composition of bismuth ferrite ($BiFeO_3$ or BFO) enables data storage capacity to increase to five times greater than the materials currently used in FeRAM production [16]. Additionally, magnetic random access memories (MRAMs) have poor writing capability [17]. The motivation of research regarding $BiFeO_3$ multiferroics is that it could lead to a new generation of memory devices that can be electrically written and magnetically read, which means the advantages of FeRAMs (ferroelectric random access memories) and MRAMs (magnetic random access memories) could be combined in a single device [17, 18]. The magnetoelectric coupling in multiferroics provides an opportunity to be used as a write scheme based on the application of a voltage rather than on large currents to reduce the writing energy of MRAMs as shown in Figure 1.2.

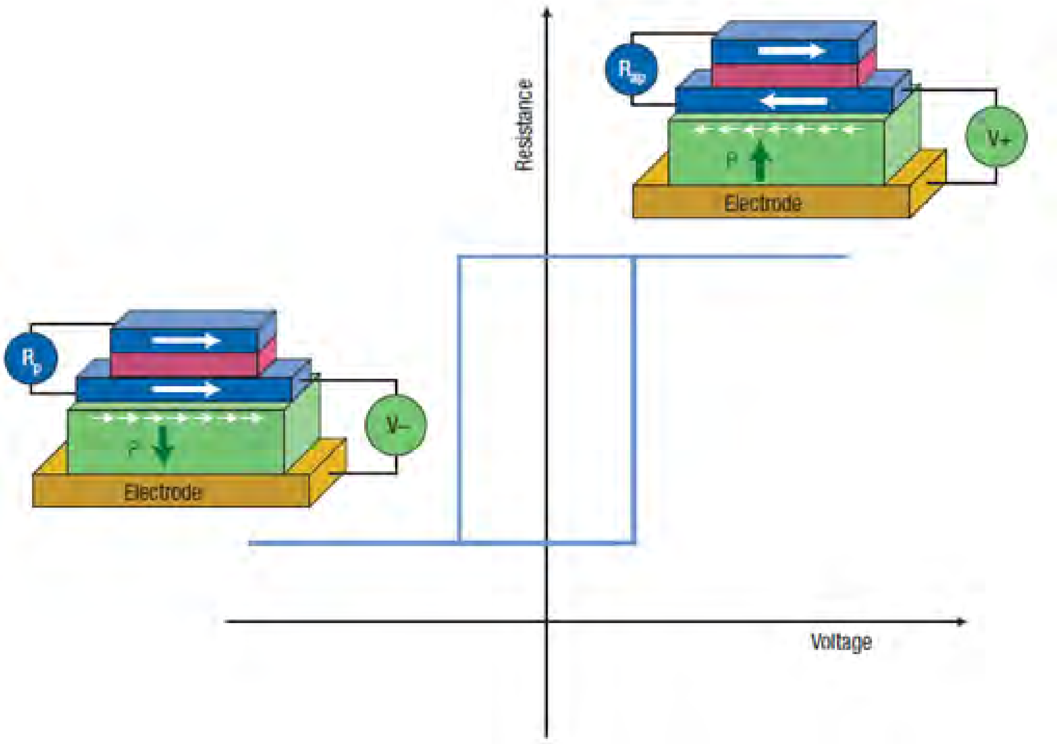

Figure 1.2: Sketch of a possible MERAM element [18]. [The binary information is stored by the magnetization direction of the bottom ferromagnetic layer (blue), read by the resistance of the magnetic trilayer (Rp when the magnetizations of the two ferromagnetic layers are parallel), and written by applying a voltage across the multiferroic layer (green). If the magnetization of the bottom ferromagnetic layer is coupled to the spins in the multiferroic (small white arrows) and if the magnetoelectric coupling is strong enough, reversing the ferroelectric polarization P in the multiferroic changes the magnetic configuration in the trilayer from parallel to antiparallel, and the resistance from Rp to antiparallel (Rap). A hysteretic dependence of the device resistance with voltage is achieved (blue curve).]

Beyond the combination of ferroic properties in a single device, the electrical control of magnetization via the magnetoelectric coupling offers the opportunity of combining the respective advantages of FeRAMs and MRAMs in the form of non-volatile magnetic storage bits that are switched by an electrical field. Indeed, although the characteristics of MRAMs equal or surpass those of alternative non-volatile memory technologies in terms of access time and endurance, they have a large handicap in their high writing energy. A possible solution for reducing the writing energy uses a spin-polarized current to reverse the magnetization of the storage layer by spin-transfer rather than magnetic fields. Spin-transfer MRAMs are currently being developed by several companies and a 2 Mb memory was recently demonstrated.

An alternative solution that could drastically reduce the writing energy of MRAMs is the use of a write scheme based on the application of a voltage rather than large currents. The magnetoelectric coupling in multiferroics provides such an opportunity. The basic operation of such magnetoelectric random access memories (MERAMs) combines the magnetoelectric coupling with the interfacial exchange coupling between a multiferroic and a ferromagnet to switch the magnetization of the ferromagnetic layer by using a voltage (Figure 1.2).

One great possible application is to use BiFeO3 as a barrier layer in spintronics. A sandwich-like structure (BFO between two ferromagnetic metals) results in tunneling magnetoresistance (Figure 1.3). This structure could be used as an electrically switchable tunnel junction, in which the ferroelectric state controls the magnetic state of the thin ferromagnetic electrodes [3].

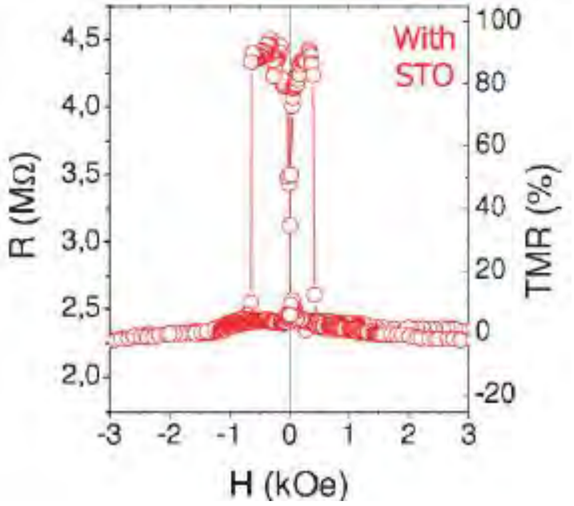

Figure 1.3: Tunneling magnetoresistance (TMR) of BiFeO3 sandwiched between (La,Sr)MnO3 and Co [3].

Another possible application of $BiFeO_3$ is its emission of THz radiation which is of great interest for many applications ranging from telecommunications to security. When a femtosecond laser pulse hits BiFeO3 films they emit THz radiation. The THz radiation is completely correlated with the poling state of the films (Figure 1.4). Furthermore, THz emission emitted by $BiFeO_3$ may be useful as an ultrafast and non-destructive method for ferroelectric memory.

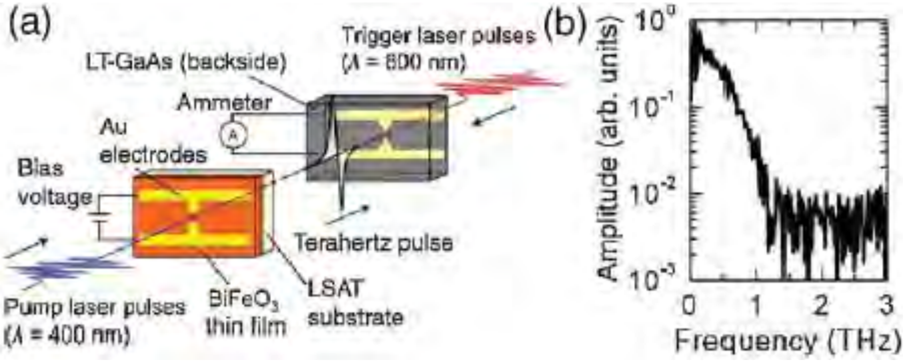

Figure 1.4: (a) Experimental setup for measuring the THz emission of $BiFeO_3$. (LT: low temperature; LSAT: $LaAlO_3$–Sr_2AlTaO_6). (b) Experimentally measured radiation [3].

The next important issue is the possibility of creating a spin valve structure. Asymmetric spin valve structures were studied by Martin et al. [19] and consist of the following different layers: Ta, CoFe, Cu, CoFe, BFO, SRO, STO, and Si(001) (Figure 1.5 a). Scanning transmission electron microscopy (STEM) was used to demonstrate the high quality nature of the heterostructure with interfaces that are very smooth and show very little interdiffusion. This allows the creation of spin valve devices using multiferroic antiferromagnets. Two switching events come from the thin and thick layers of CoFe. Also, a negative shift of the hysteresis loop by 40–50 Oe was observed (Figure 1.5 b). Thus, it has been demonstrated that $BiFeO_3$ can also be used for the construction of device structures such as spin valves.

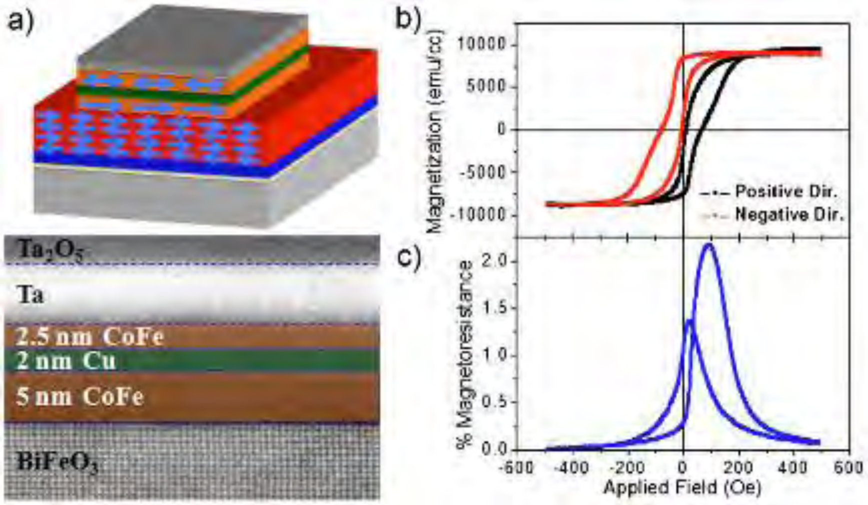

Figure 1.5: Spin valve structures based on CoFe/Cu/CoFe/BFO heterostructures. (a) Schematic illustration and scanning transmission electron microscopy image. (b) Magnetic hysteresis loops of spin valve structures. (c) Current-in-plane magnetoresistance measurements [19].

Several issues should however be solved before realization in devices. The problems are high leakage current density and very low magnetic moment. The spiral spin structure that cancels macroscopic magnetization and inhibits the linear magnetoelectric effect in bulk bismuth ferrite Many attempts have been made to enhance the ferroelectric and ferromagnetic properties of BiFeO$_3$. The current research deals with improvement of magnetic properties by controlling particle size of the synthesized BiFeO$_3$ nanoparticles.

1.4 Aims of the research

The main aims of this research include:

(i) To synthesize BiFeO$_3$ nanoparticles at relatively low temperature via a soft chemistry route.

(ii) To obtain pure nanocrystalline BiFeO$_3$ phase by washing with acetic acid instead of nitric acid.

(iii)To study thermal decomposition behavior of BiFeO$_3$ precursor xerogel.

(iv) To investigate thermodynamic stability, structure and formation of $BiFeO_3$ phase with increasing temperature.

(v) To examine microstructure and establish a comprehensive particle size-magnetic property relationship of synthesized $BiFeO_3$ nanoparticles.

1.5 Current Research trends on $BiFeO_3$:

The current section briefly describes different synthesis techniques, basic properties and possible applications of nanostructures such as thin films and nanoparticles.

1.5.1 Thin films

The appearance of new thin-film growth techniques has allowed the creation of high-quality thin-film samples. In conjunction with analytical tools, it has become possible to design novel nanodevices based on magnetoelectric coupling. The most often used thin-film growth techniques are:

- Pulsed laser deposition (PLD);
- RF magnetron sputtering;
- Chemical vapor deposition (CVD) and metal-organic CVD (MOCVD);
- Chemical solution deposition (sol-gel);
- Molecular beam epitaxy (MBE).

Pulsed laser deposition (PLD) is a method used to produce thin films by using a laser ablation technique. Figure 1.6 briefly describes the principle of PLD.

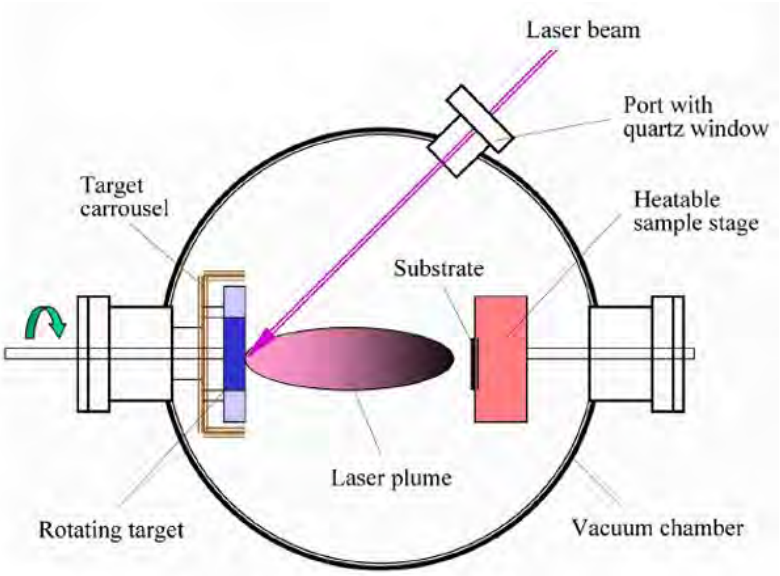

Figure 1.6: The principle of PLD.

Wang [20] was the first to study $BiFeO_3$ films using the PLD technique. It is well known that substrates greatly influence the properties of thin films that are grown on them. The substrates most often used to grow $BiFeO_3$ using the PLD technique are Si, $SrTiO_3$(STO) and $DyScO_3$ [21, 22]. It is noted that in this case, thin films with thicknesses ranging from 2 to 600 nm (Figure 1.7) [21] were obtained by the PLD technique.

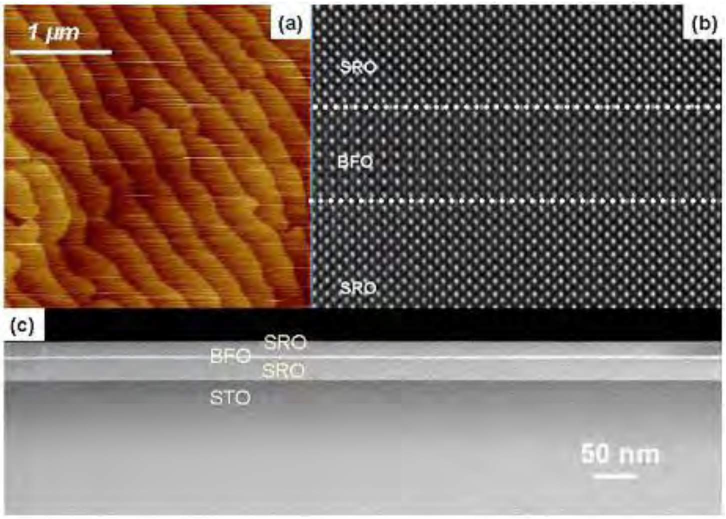

Figure 1.7: (a) AFM image of a SRO/BFO/SRO heterostructure, and typical (b) high magnification and (c) low magnification STEM images of a 3 nm thick BFO film [21].

In the case of the $SrTiO_3$(STO) substrate, the resultant crystal structure also depends on the orientation of the substrate. When grown on either (100)- or (101)- oriented $SrTiO_3$ substrates,

$BiFeO_3$ has monoclinic symmetry; the rhombohedral structure is obtained only if films are grown on (111) oriented $SrTiO_3$ substrates [22]. Ferroelectric hysteresis loops have been observed for such thin films, indicating ferroelectric behavior [20-22]. Measurements of the polarization of these films show an enhancement of the spontaneous polarization in the strained films [20, 22]. In the case of the $SrTiO_3$ substrate, a room temperature spontaneous polarization of 50–60 µC/cm2 was obtained, almost an order of magnitude higher than that of the bulk (Figure 1.8) [20].

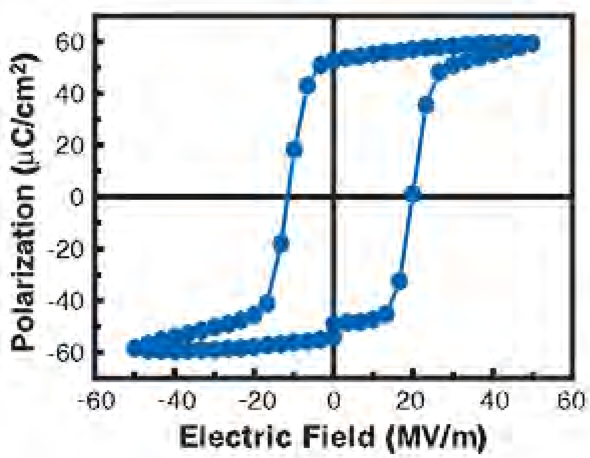

Figure 1.8: Ferroelectric hysteresis loop for BiFeO3 grown on (100) oriented SrTiO3 substrate [20].

Figure 1.9 presents a magnetic hysteresis loop measured on a 70-nm thick $BiFeO_3$ film [20]. The graph shows a high saturation magnetization of ~150 emu/cm^3 and a coercive field of ~ 200 Oe. The graph also shows the in-plane and out-of-plane magnetization loops.

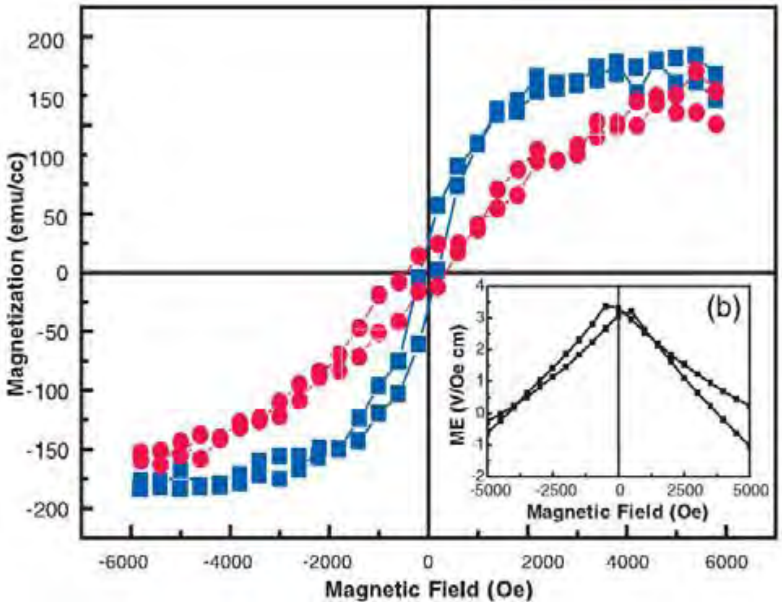

Figure 1.9: Magnetic hysteresis loop for a 70-nm thick BFO film. The in-plane loop is shown in blue, and the out-of-plane loop is in red [23].

RF-magnetron sputtering is a method that allows the growth of extremely smooth surfaces. Another of its advantages is a reduction in the risk of device damage due to interdiffusion and chemical fluctuations. The off-axis radio frequency magnetron sputtering technique is schematically shown in Figure 1.10.

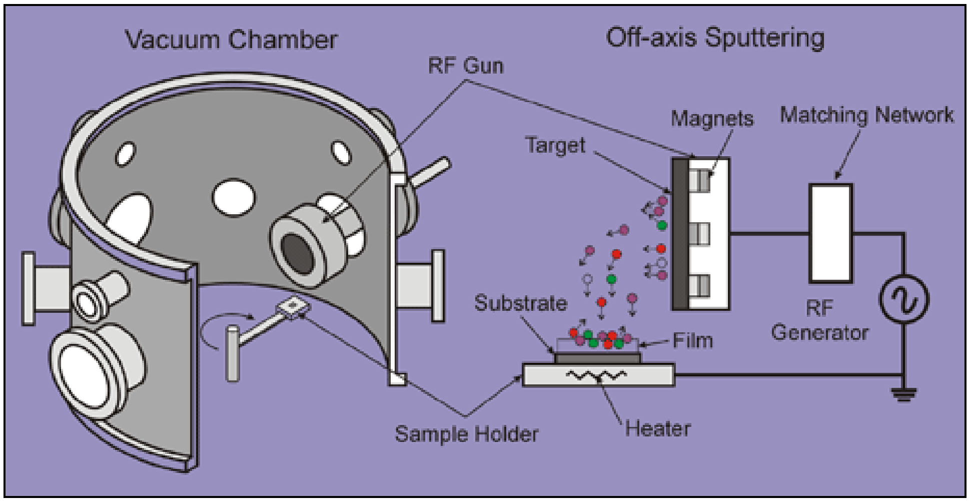

Figure 1.10: Schematic view of magnetron sputtering process.

Two types of substrates (Si and $SrTiO_3$) have been used to grow $BiFeO_3$ films by rf-magnetron sputtering [24, 25]. In the case of the Si substrate, a buffer layer of $Pt/TiO_2/SiO_2$ was used and films ranging in thickness from 85 to 400 nm were made [24]. The surface morphology of the BFO films grown on $Pt/Ti/SiO_2/Si$ substrates was determined by atomic force microscopy (AFM) and is shown in Figure 1.11.

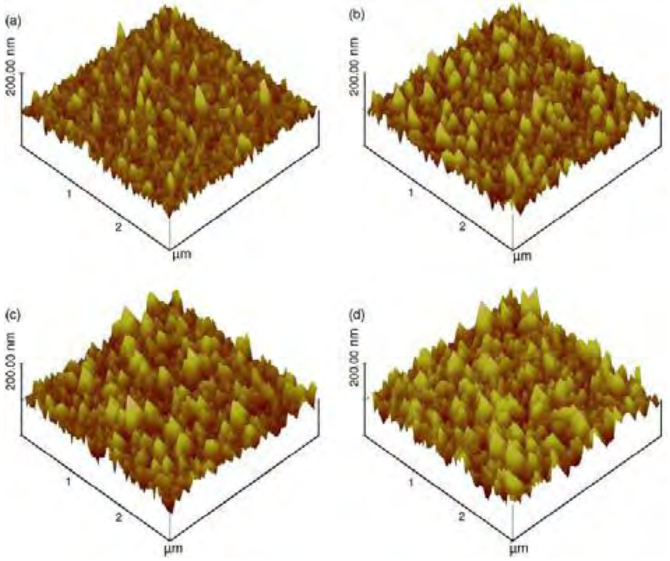

Figure 1.11: AFM images of BFO films with different thicknesses :(a) 85 nm, (b) 120 nm, (c) 210 nm, and (d) 280 nm [25]. The substrate is Pt/Ti/SiO2/Si.

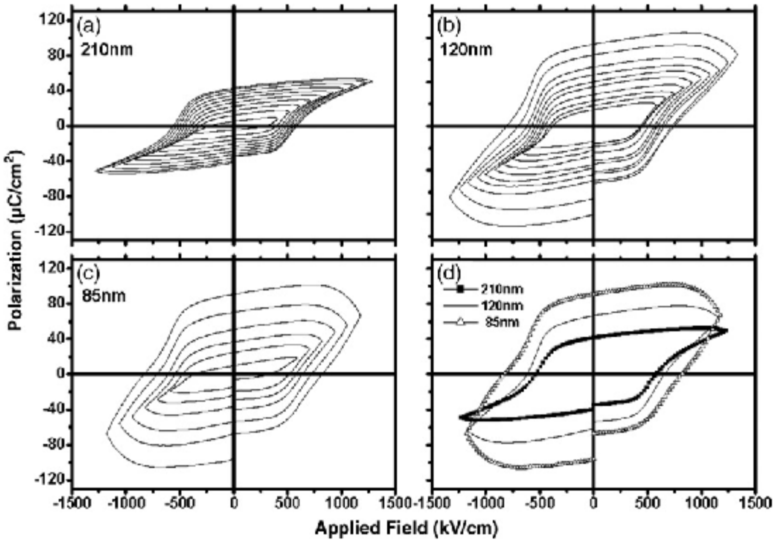

Figure 1.12 Polarization (P)–electrical field (E) hysteresis loops determined for BFO films at room temperature with thickness (a) 210 nm, (b) 120 nm, and (c) 85 nm. (d) P–E loops for BFO films measured up to 1200 kV/cm [25]. The substrate is Pt/Ti/SiO2/Si.

Figure 1.12 shows the polarization–electrical field (P–E) hysteresis curves of the BFO thin films with different thickness. The remnant polarization (Pr) and coercive field (Ec) both increase with decreasing film thickness. The existence of leakage currents hinders the precise determination of Pr and Ec. More saturated P–E hysteresis curves were obtained for the BFO film with thickness 210 nm than for the other two films. Thus, a thicker BFO film possesses a more saturated P–E hysteresis loop. The values of (Pr, Ec) were (41.6, 570), (66.8, 650) and (90.6 µC/cm^2, 820 kV/cm), for BFO films of thickness 210, 120 and 85 nm, respectively, under an electric field of 1200 kV/cm [25]. Some authors believe that the source of the apparent enhancement of ferroelectric properties is strain effects in as-grown epitaxial films, while others believe that confinement effects are important. However, the effects of such phenomena are still unclear and a major concern is still the quality of the thin films.

To summarize, in this section we have compared different thin film growth techniques. Several different types of substrates (Si, $SrTiO_3$, $SrRuO_3$) can be used to grow high quality films. The different techniques give similar values of remnant ferroelectric polarization for films grown on the same substrates. However, the different techniques allow different means by which to control the quality of the films. We note that the recently obtained [21] high remnant ferroelectric polarization measured for a $BiFeO_3$ single crystal should be taken into account when considering whether thin films give an enhancement of the ferroelectric properties.

Another important technique is the chemical solution deposition (CSD) or sol-gel process. CSD involves the formation of a sol followed by gelation to form a gel. A sol is a colloidal suspension and a gel is a network in a continuous liquid phase. Figure 1.13 briefly describes the essential sol-gel processing steps. CSD is used primarily for the fabrication of metal oxide structure. The sol-gel process is cheap and simple and is able to produce stoichiometrically accurate crystalline films.

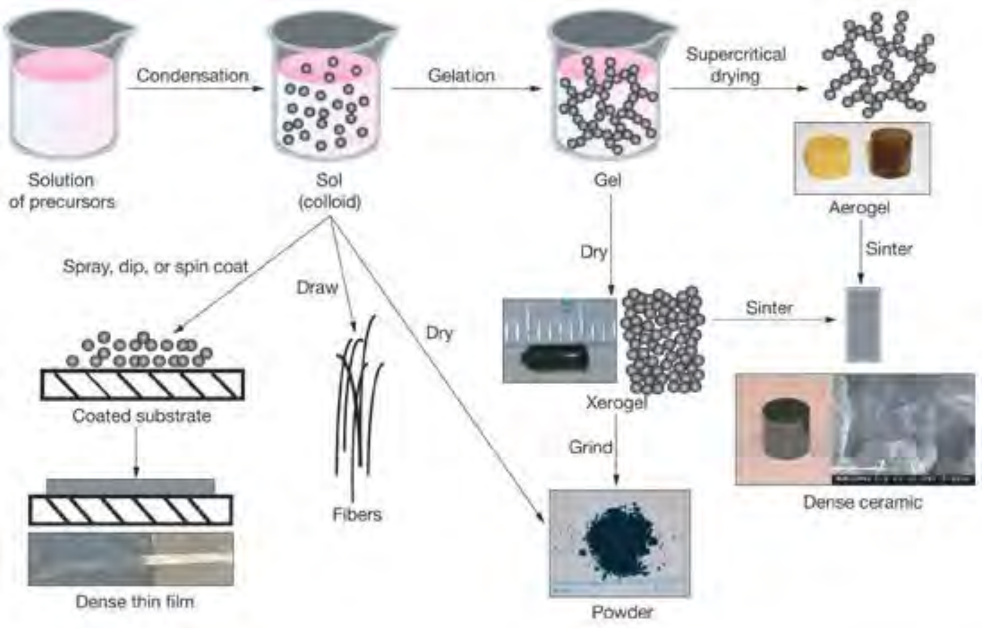

Figure 1.13: Principle of chemical solution deposition (CSD) or sol-gel method.

The CSD method has successfully been used to create $BiFeO_3$ thin films with a wide range of thicknesses from 80 to 1200 nm [26,27]. A silicon-based substrate (Pt/Ti/SiO2/Si) is usually used to deposit $BiFeO_3$ films [27]. The microstructures and surface morphologies of the films were examined using SEM (Scanning Electron Microscopy), AFM (Atomic Force Microscopy), and AES (Auger Electron Spectroscopy). Figure 1.14 shows an AFM image of the surface topography of a $BiFeO_3$ thin film annealed at 500°C for 1h, which reveals an extremely smooth surface.

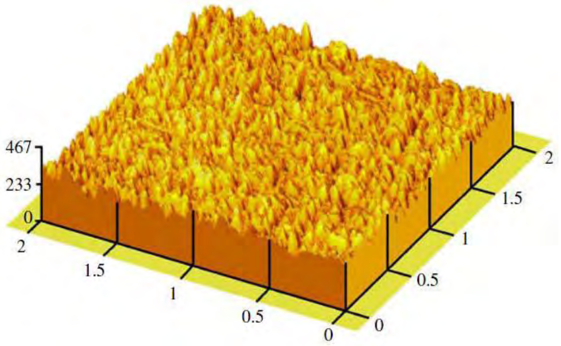

Figure 1.14: AFM image of polycrystalline BFO thin film annealed at 500°C [26].

The remnant polarizations were 92, 84, and 68 μC/cm^2 for 400, 300, and 180 nm-thick films, respectively. The large remnant polarization and low leakage current of this film are particularly suitable for high-density FeRAM devices, and the large piezoelectric coefficient shows that $BiFeO_3$ is also well-suited to applications such as actuators and micro electromechanical systems (MEMS). Moreover, $BiFeO_3$ films have potential as sensing devices and they can covert mechanical vibration energy into electrical energy, which may be utilized for micro biosensors

1.5.2 Nanoparticles:

Nanomaterials are fundamentally interesting not only because they are small but also because they possess fascinating size-dependent optical, electronic, thermal, mechanical, chemical, and catalytic properties, which are potentially distinct from their bulk counterparts as well as from the atomic or molecular precursors from whence they were derived [28]. This unique chemical and physical behavior of nanomaterials can in general be ascribed to an increased relative surface area and the dominance of quantum effects. These two factors are interrelated because the surface-to-volume (S/V) ratio dramatically increases as particle size decreases.

As a particle decreases in size, a greater proportion of atoms is found at the surface as compared with that inside the core of a particle. For a spherical particle, the S/V ratio is inversely proportional to its radius, R ($S/V = (4\pi R^2)/(4/3\cdot\pi R^3) = 3/R$). For example, a particle built up by hexagonal or cubic close-packed atoms measuring 30 nm in diameter possesses 5% of its atoms on its surface. A 10 nm-sized nanoparticle possess 20% of its atoms on its surface, whereas a 3 nm-sized nanoparticle has 50% of its atoms on its surface. Thus, nanoparticles maintain a much greater surface area per unit volume as compared with bulk. Surface atoms are chemically more active (in other words, less stable) as compared with core atoms due to their relative lack of coordination with other atoms and also due to the presence of unsaturated sites or dangling bonds. In fact, it is generally accepted that the property of a matter depends strongly on the surface atoms of a materials. Thus, a greater surface area per unit volume ratio is anticipated to result in greater, enhanced reactivity for the unit system.

For crystalline solids, as the size of their structural components decreases, there is a much greater interface area within the solids, which can greatly affect both their mechanical and electrical properties. For example, most metals are composed of relatively small crystalline grains; the boundaries between the grains can arrest the propagation of defects when the solid is stressed, thus providing for the metal‟s hardness.31 Moreover, nanoscale crystalline solids may contain unusual forms of structural disorder (*e.g.*, bond length contractions, random disorder, and a type of disorder characterized by correlated atomic displacements) that can substantially modify a material‟s properties [29]. Moreover, a nanoparticle structure possessing internal strain, which results from lattice contraction and disorder, can noticeably modify the electronic properties of nanoscale analogues of crystalline solids, such as with ZnS [29].

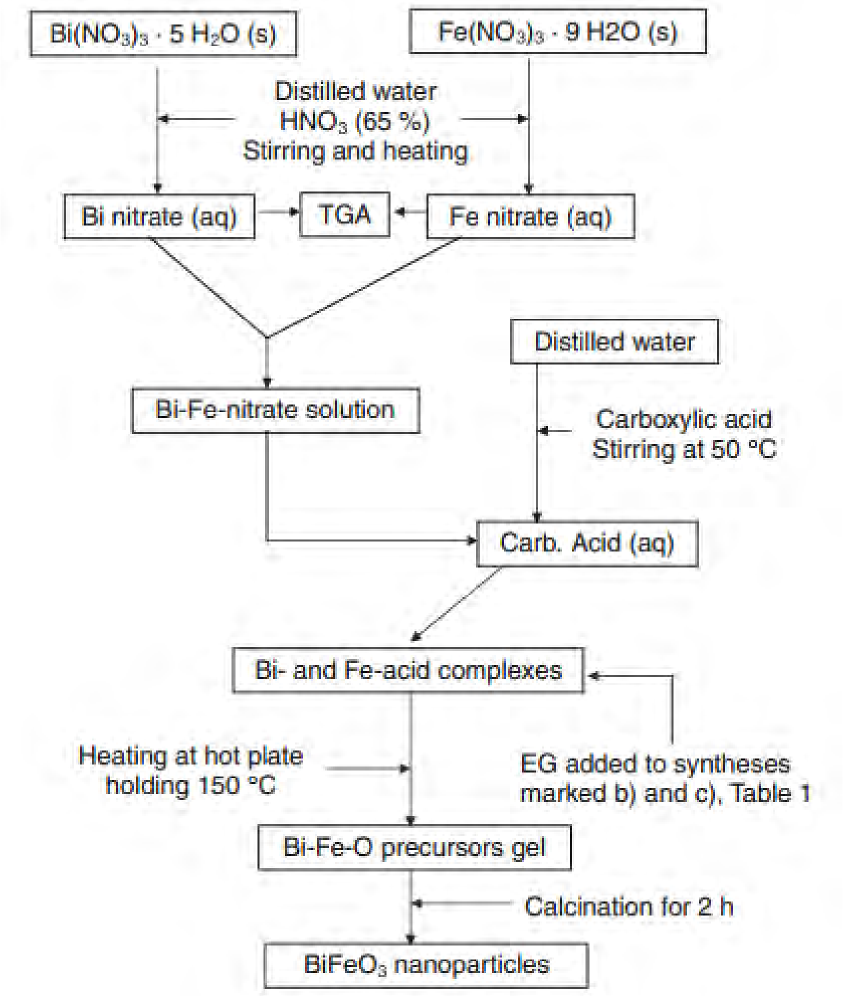

Figure1.15: Scheme of Pechini sol-gel synthesis routes for $BiFeO_3$

Recent approaches have focused on developing novel structures such as zero-, one-, and two-dimensional nanostructures of $BiFeO_3$. Up to now, several wet chemical routes (co-precipitation, hydrothermal, solvothermal, sonochemical, sol-gel and combustion) have been developed for the synthesis of $BiFeO_3$ powders [30-34]. The most convenient methodology used to produce nanoparticles is variations of the sol-gel technique (mostly Pechini technique). These methods allow the synthesis of particles ranging in size from less than 15 nm to greater than 100 nm.

The Pechini method belongs to the sol–gel category of fabrication methods. In this method, an a-hydroxy carboxylic-containing compound forms a polybasic acid chelate with metal cations; which successively polymerize with a polyhydroxy alcohol. After calcination process, nanometer-sized powders are achieved. When compared to other sol-gel methods, the Pechini method has better compositional homogeneity, lower toxicity and lower cost. The method‟s advantages include its relative simplicity. A Pechini sol-gel synthesis route is shown in Figure 1.15.

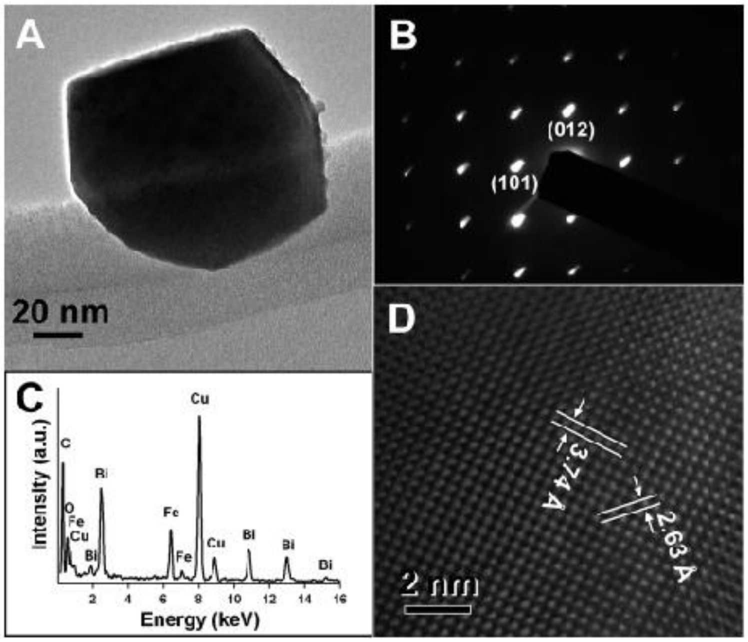

Figure 1.16: TEM image (a) and SAED pattern (b) of a BiFeO3 nanoparticle (95 nm) generated using an annealing temperature of 600 °C, and its corresponding EDS (c). The Cu and C peaks originate from the TEM grid. (d) HRTEM image of a typical portion of the $BiFeO_3$ nanoparticle [35].

$BiFeO_3$ nanoparticles with diameters of the order of 62 nm or smaller (the wavelength of the intrinsic spiral modulated spin structure), show strong size-dependent effects. A transmission electron microscopy (TEM) image of a $BiFeO_3$ nanoparticle synthesized using the sol-gel method is shown in Figure 1.16.

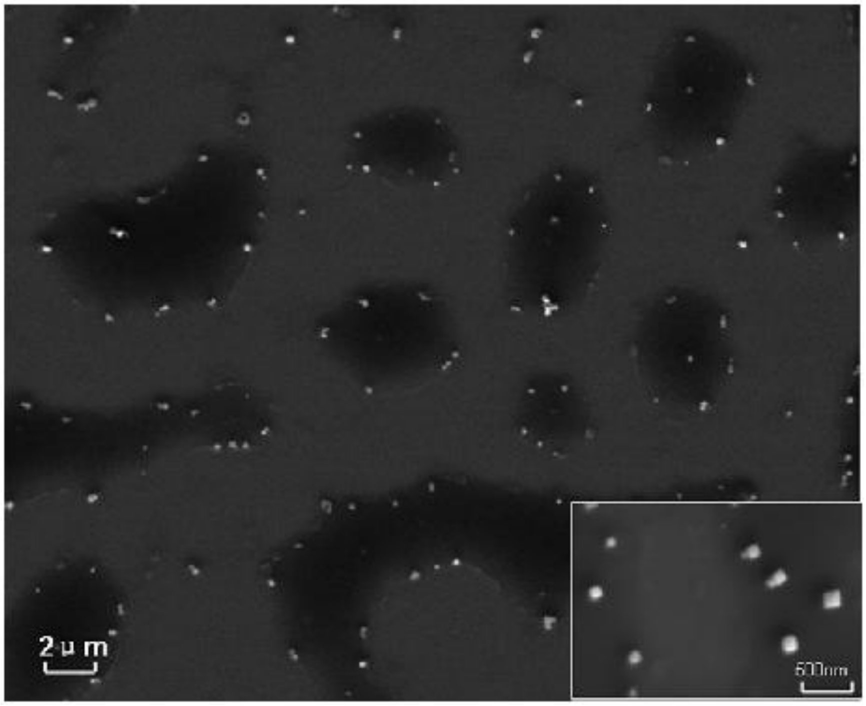

Figure 1.17: SEM image of $BiFeO_3$ nanoparticles sintered at 600° C [36].

An SEM image of $BiFeO_3$ nanoparticles sintered at 600 C (Figure 1.17) shows that they are homogeneous and welldefined. The inset to Figure 1.17 is a high-magnification SEM image showing that the $BiFeO_3$ nanoparticles lie in the size range 110–160 nm and have cubic morphology [36]. Magnetic measurements were performed on these nanoparticles as well as on bulk $BiFeO_3$ (Figure 1.18). The magnetic response increases as the size of the as-prepared $BiFeO_3$ nanoparticles decreases.

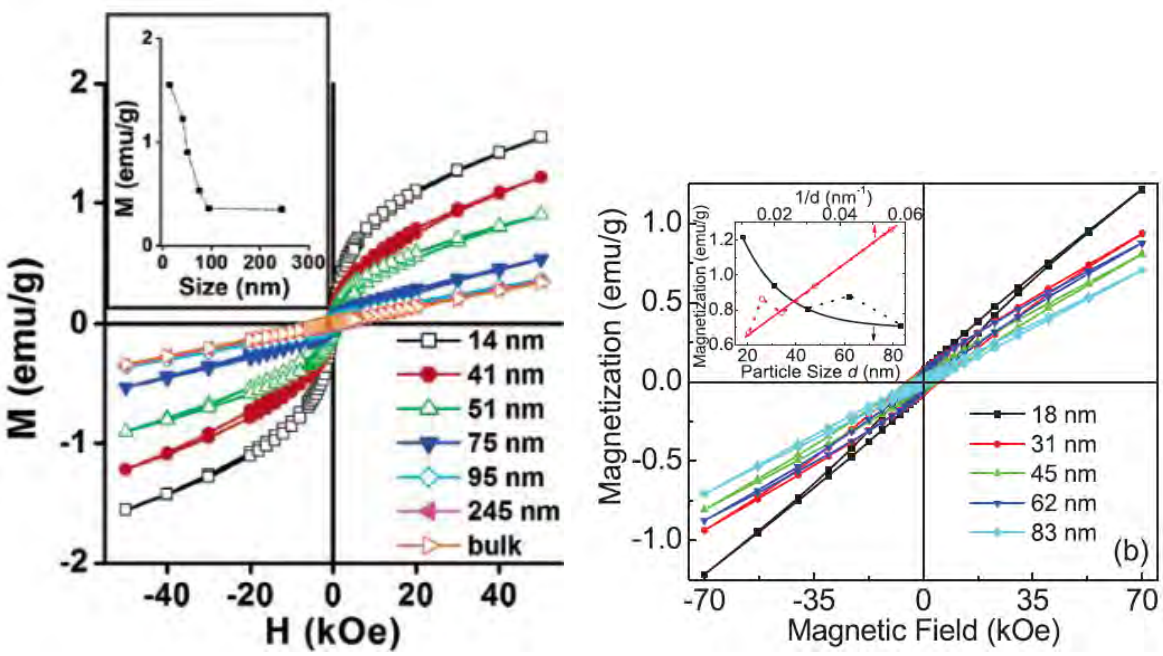

Figure 1.18: *Hysteresis* loops at 300 K for BiFeO3 nanoparticles with indicated sizes [35,37].

Moreover, the magnetic properties of $BiFeO_3$ nanoparticles with a mean size of 245 nm are very similar to those of the bulk. The results presented in Figure 1.18 imply that a magnetic response in $BiFeO_3$ is initiated when the size of the system is less than~ 62 nm. The magnetic response of $BiFeO_3$ nanoparticles greatly increases for samples below 62 nm (the period length of the spiral modulated spin structure of $BiFeO_3$), as compared with the bulk. The authors of [35] believe that this magnetic moment can be explained as a result of frequently interrupted antiferromagnetic ordering at the particle surface. The relative proportion of uncompensated spins at the surface becomes larger with decreasing particle size. Hence, the nanoparticles show size-dependent magnetic behavior according to confinement effects. However, other theories such as interruption of the spiral modulated spin structure, strain effects, and material quality, should also be taken into account.

1.6 Targets and challenges of this thesis:

The main focus of this research is to improve room temperature ferromagnetic properties of $BiFeO_3$ by controlling particle size of the synthesized nanoparticles. We expect size controlled synthesis of pure $BiFeO_3$ nanoparticles at relatively low temperature via a modified Pechini sol-gel route. But synthesis of pure $BiFeO_3$ is very difficult because the temperature stability range of single phase $BiFeO_3$ is very narrow. Various impurity phases have been reported to occur, mainly comprising of $Bi_2Fe_4O_9$ and $Bi_{25}FeO_{40}$. Presence of such impurities results in high leakage current and poor ferroelectric hysteresis behavior. Usually a strong acid (HNO_3) is used to remove the secondary phases that are formed during synthesis of $BiFeO_3$ nanoparticles. But HNO_3 may dissolve the $BiFeO_3$ phase [38]. So CH_3COOH, a week acid was used for washing purpose in this research.

However controlling particle size and shape of nanoparticles is critical. Final properties depend on the microstructure and homogeneity of the synthesized powders. Irregular shape of the particles has higher demagnetization factor and lower saturation magnetization. In these work we target uniform particle size and shape of the synthesized particles to improve magnetic properties. Ethylene glycol would be a potential candidate to modify the sol-gel chemistry to improve particle morphology of the synthesized powders.

CHAPTER 2

LITERATURE REVIEW

2.1 Introduction

Maxwell‟s equations [39] that govern the dynamics of electric fields, magnetic fields and electric charges, show that the magnetic interactions and motion of charges are intrinsically coupled to each other. These equations tell us about the unified nature of magnetism and electricity [39]. It is to be noted that there are numerous similarities (e.g. their behavior in the external fields, anomalies at a critical temperature, their domain structures) in the thermodynamics of ferroelectrics and ferromagnet; which is also expected if one looks at the equivalence of equations of electrostatics and magnetostatsics in polarizable media. These similarities are particularly striking in view of the seemingly different origins of ferroelectricity and magnetism in solids- (a) as is known, magnetism is related to ordering of spins of electrons in incomplete ionic shells (b) whereas, ferroelectricity results from relative shifts of negative and positive ions that induce surface charges. There are, however cases where these degrees of freedom couple strongly. For example, for spintronic materials at large fields, the effects of spins on the transport properties of solids (and vice versa) allow the possibility to control one by other.The quest for these materials are propelled by the prospect of controlling charges by applied magnetic field and spins by applied voltages, to construct new forms of multifunctional devices.

2.2 Multiferroics

2.2.1 Classification of ferroics:

Ferroics are an important class of technological materials with unique properties that make them the leading candidates in many modern technologies such as electronics, data storage, sensing, communications and medicine. The word ferroics is derived from "ferrum", the Latin word for iron which is the oldest known ferroic material. At room temperature, iron displays a permanent magnetic moment which can be reversibly switched with an external magnetic field. Such a unique property is a characteristic of a class of materials known as ferromagnetics. Other examples of ferroic materials are ferroelectrics, which present a spontaneous, switchable intrinsic lattice polarization and ferroelastics, which can be reversibly deformed under the action of an external mechanical stress. A common feature shared by ferroic materials is their ability to undergo a phase transition from a non-ferroic to a ferroic state. For ferromagnetic and ferroelectric materials, this phase transition occurs at a well-defined temperature known as the Curie temperature. The symmetry of the ferroic crystal is lowered at the Curie temperature and this is accompanied by a huge variation in the ferroic property (polarization or magnetization) associated with the material.

2.2.2 Ferroelectric materials

Ferroelectricity (FE) was first discovered in Rochelle salt in 1921. At that time, it was called Seignette-electricity, honoring its discoverer. For the past few decades, ferroelectric materials have received a great amount of interests because of their various uses in many applications such as nonvolatile ferroelectric random access memories (NVFRAM), dynamic random access memories, sensors and micro actuators [40].

A crystal is said to be ferroelectric when it possesses at least two equilibrium orientations of the spontaneous polarization vector in the absence of an external electric field, and the spontaneous polarization can be switched between those orientations by an electric field. The polar character of the orientation states should represent an absolutely stable configuration in a null field.

It is well known that crystals can be classified into thirty-two crystal classes (point groups) according to the symmetry elements they possess. Among these thirty-two crystal classes, eleven of them are characterized by the existence of a center of symmetry: they are thus centrosymmetric. A centrosymmetric crystal cannot posses any polar properties. The remaining twenty-one crystal classes do not have a center of symmetry; thus, it is possible for them to (i) have one or more polar axes, (ii) possess odd-rank tensor properties. With one exception, all non-centrosymmetric point groups exhibit piezoelectric effect that is defined by a change in electric polarity under applied stress, and vice versa, that is the converse piezoelectric effect.

Out of the twenty piezoelectric classes, ten possess a unique polar axis. Crystals in these classes are called polar because they are spontaneously polarized. The value of the spontaneous polarization depends on temperature. When temperature changes, a change in the polarization occurs and electric charges can be observed on those crystal faces perpendicular to the polar axis. This is called the pyroelectric effect. The ten crystal classes with a unique polar axis are also called pyroelectric classes. Ferroelectric crystals belong to the pyroelectric family, but they only constitute the part that the direction of the spontaneous polarization can be reversed by external electric field.

So, a (proper) ferroelectric possesses a spontaneous polarisation of the electric dipole due to a lack of inversion symmetry within the crystal structure. For example, consider the most extensively studied and widely used classic perovskite of the form ABO_3, in which a central positive B-ion (a transition metal element) is surrounded by an octahedron of negatively charged oxygen ions (Figure 2.1). A shift in the position of the B-site ion would break the inversion symmetry and cause the induction of a dipole moment, giving rise to ferroelectric order. Such shifts can occur during structural phase transitions, in which the system moves from a high to low symmetry state (e.g. cubic to tetragonal). In the majority of ferroelectric perovskites, the B-site atom has an empty d electron shell, which allows covalent bonding with the full p orbitals of the oxygen atoms. One of the best known examples of a proper ferroelectric is $BaTiO_3$. As shown in Figure 2.1, the Ba^{2+} cations are located at the corners of the unit cell. A dipole moment occurs due to relative displacements of the Ti^{4+} from their symmetrical positions.

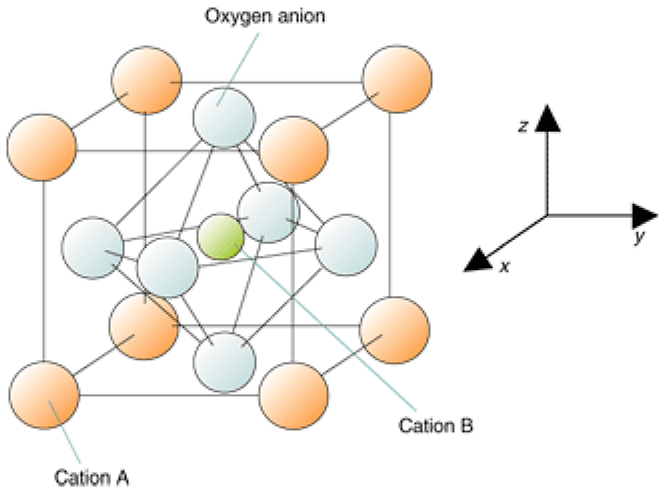

Figure 2.1: Perovskite crystal structure, showing a dipole moment generated by a displaced B-site atom.

Ferroelectricity can also occur due to the existence of lone pairs of electrons on the outer shell of the A-site atom, which are highly susceptible to polarisation. This is the cause of ferroelectricity in $BiFeO_3$. Whether A-site or B site polarization would occur depends on Goldschmid Tolerance Factor, $t=(r_{A\text{-site}}+r_O)/\sqrt{2}(r_{B\text{-site}}+r_O)$; where t >1 results in A-site polarization.

In an improper ferroelectric, the spontaneous polarisation is not due to a polar displacement of the ions, but occurs as a result of some other effect within the material. In a geometric ferroelectric, the dipole moment occurs due to non-polar lattice distortions, due to e.g. electrostatic forces rather than changes in chemical bonding. An example of this is in $YMnO_3$, where a ferroelectric state is due to a buckling of the rigid MnO_5 bipyramids. In charge ordered ferroelectrics, the spontaneous polarisation is dependent on electron correlations in the material. Such charge ordered ferroelectricity is observed in $LuFe_2O_4$. Improper ferroelectricity can also occur due to magnetic order.

2.2.3 Ferro-, antiferro-, and ferri-magnetic materials

The phenomenon of magnetism has been known to mankind for many thousands of years. Lodestone (Fe_3O_4) was the first permanent magnetic material to be identified and studied. The magnetic moment of an atom/ion has three principal sources: (1) the spin of electrons; (2) electron orbital angular momentum about the nucleus; and (3) a change in the orbital moment induced by an applied magnetic field. The first two effects give paramagnetic contributions to the magnetization, and the third gives a diamagnetic contribution [41].

In a crystal, the overall magnetic property depends on two factors: (i) the magnetic moment associated with each atom/ion, and (ii) the interactions between these magnetic moments. In the case that there are no unpaired electrons around each atom/ion, there will be no net magnetic moments associated with them (bearing in mind that both orbital moments and electron spins cancel to zero in a fully filled orbital), the material will show diamagnetic behavior. When there are unpaired electrons, every atom/ion has a net magnetic moment and depending on the interactions between the magnetic dipoles, the material may show (i) paramagnetism (PM); (ii) ferromagnetism (FM); (iii) antiferromagnetism (AFM) and (iv) ferrimagnetism (FIM). In a paramagnetic material, alignment of adjacent moments is observed only under applied magnetic field. Ferromagnetism consists of parallel aligned adjacent moments. Antiferromagnetic order consists of antiparallel aligned equal moments. And, ferrimagnetic order consists of antiparallel unequal moments, resulting in a non-zero net magnetization.

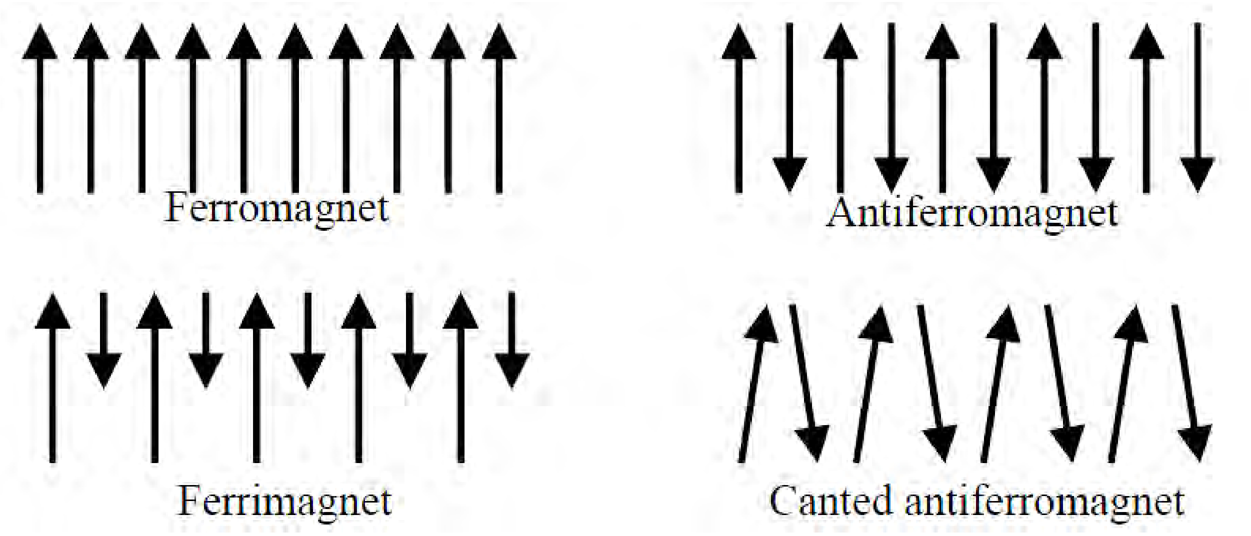

Figure 2.2: Common examples of magnetic dipole ordering.

Ferromagnetism is a very strong magnetic response compared with paramagnetic and diamagnetic behaviors. It is characterized by a transition temperature (Neel temperature, T_N).Above this temperature, the material is paramagnetic. Below this temperature, it is ferromagnetic.

A material‟s magnetic property can be understood from the M or B versus H curves, called the magnetization curves.

The magnetic induction (B) is the response of a material to the applied magnetic field (H). The relationship between B and H depends on the material; The magnetization (M) is defined as the magnetic moment per unit volume such that,

$$M = \chi . H \text{ and } B = \mu . H; \chi = \text{susceptibility and } \mu = \text{permeability}$$

From Figure 2.3a, we observe that the net magnetization of diamagnetic, paramagnetic and antiferromagnetic materials is very low even at a very high applied magnetic field and the relationship between M and H is linear. But, in ferromagnetic and ferrimagnetic materials, even at a low applied magnetic field, the value of magnetization is very high. Moreover, the M − H curve is non-linear, and the magnetization saturates at higher values of H as shown in Figure 2.3b.

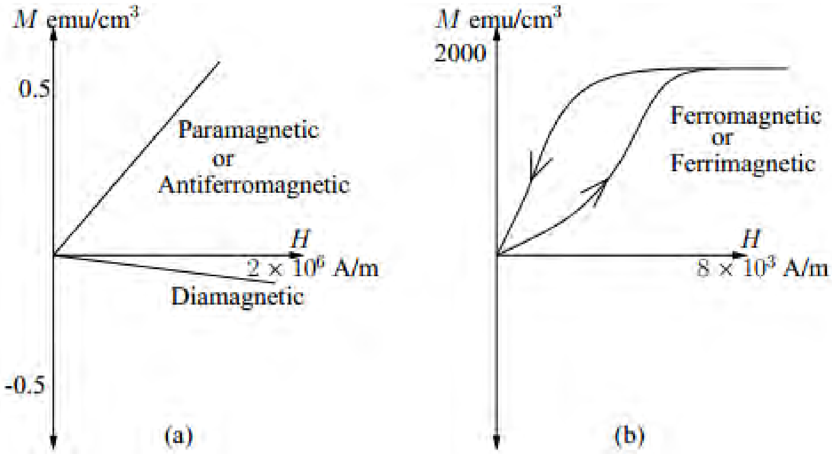

Figure 2.3: M-H curves for (a) diamagnetic, paramagnetic, antiferromagnetic (b) ferromagnetic and ferromagnetic materials. (N.A. Spaldin 2003)

All ferromagnetic and ferrimagnetic materials exhibit the phenomenon of hysteresis as shown in the four quadrant hysteresis loop in Figure 2.4. The performance of any magnetic material can be defined with the help of this hysteresis loop. M_S is the saturation magnetization and is a measure of how strongly the material can be magnetized. M_r is the remanent magnetization which is the residual, permanent magnetization left after the removal of the applied field. In order to demagnetize the specimen from its remanent state, a reverse field H_c, the coercive field is required to reduce the residual magnetization to zero. Higher the value of H_c, larger is the retaining capacity of the material. This is the reason that, the PL in an MTJ is with a larger coercivity, so that it requires a larger field to change its magnetization than the FL. Even ferromagnetic materials become paramagnetic, with random orientation of moments, above Neel temperature, T_N.

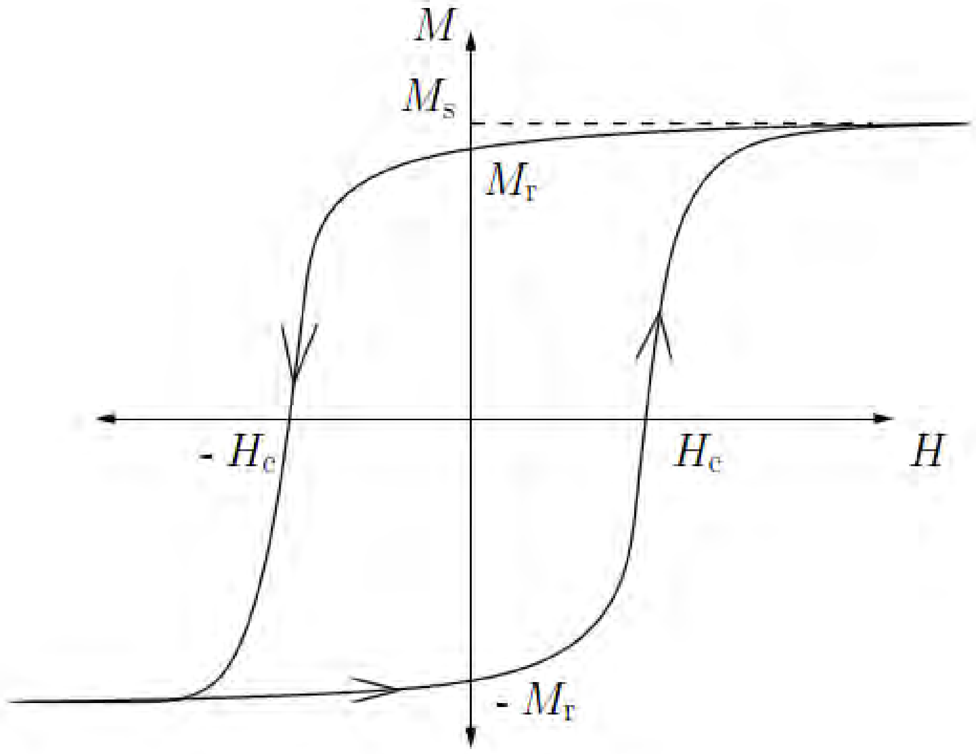

Figure 2.4: M-H curves for ferromagnetic and ferrimagnetic materials.

2.2.4 Ferroelastic material

Ferroelastic materials develop a spontaneous strain below a phase transition temperature. From the symmetry point of view, the material undergo a structural phase transition from a high symmetry phase to a low symmetry phase, which is characterized by a „broken symmetry" of the high symmetry phase [42].

The phase transition mechanism results in a spontaneous strain. The spontaneous strain can be quite large. For example, the spontaneous strain of a typical ferroelastic material is >2%. The correlated changes in the enthalpy of the crystal related to this formation of spontaneous strain often reach some 6 KJ/mole, an energy which would reactive equivalent changes in thermochemical phase diagrams of some hundreds of degrees in temperature. In order to release the energy created by the phase transition, a twin domain structure is often created within a ferroelastic crystal, where the dominant twin planes are oriented approximately perpendicular to each other.

A wall between two adjacent domains can be envisaged as an internal surface of the crystal. The orientation of an individual twin wall is then determined by the condition that the crystal in the low-symmetry phase tends to maintain the total symmetry of the high-symmetry phase as an average. The domains are related equivalent to each other via the symmetry element lost at the phase transition that give rise to the long-range ordered state. It is commonly accepted that stress induced domain wall motion in ferroelastic materials yield hysteretic macroscopic behavior. Mueller et al. [43] showed that nonlinear effects in ferroelastic crystals are related to the properties of ferroelastic domain walls pinned on defects, which became de-pined above a critical stress level. Additionally, Jian and Wayman [44] observed domain wall motion in single-crystal and polycrystalline $LaNbO_4$ ferroelastics under stress, and argued that the nonlinear elastic behavior is a direct result of domain wall motion, rather than the intrinsic properties of the crystal. In addition, Newnham [45] concluded that stress-induced movement of domain walls is the principle source of hysteresis in ferroelastics. Figure 2.5 illustrates the stress-induced twin movement of a ferroelasteic $Pb_3(Pb_4)_2$ crystal [43].

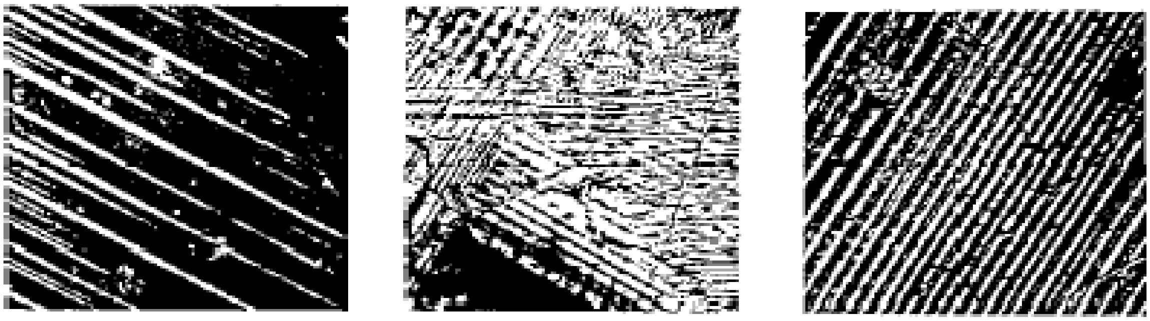

Figure 2.5: Experimentally observed microstructures of lead phosphate. [The two fully „switched" crystals (a) and (c) display striped twin patterns whereas the crystal in the intermediate state (b) shows superposition of various twin orientations.]

2.3 Order parameter couplings

There are four order parameters. The order parameter couplings are given below:

- **Piezoelectricity:** describes a change in strain as a linear function of applied electric field, or a change in polarization as a linear function of applied stress.

- **Piezomagnetism:** describes a change in strain as a linear function of applied magnetic field, or a change in magnetization as a linear function of applied stress.

- **Magnetoelectricity:** describes the influence of a magnetic (electric) field on the polarization (magnetization) of a material.

- **Electrostriction:** describes a change in strain as a quadratic function of applied electric field.

The effects of cross-coupling between ferroic orders is, represented in figure 2.6. Changes in strain as a function of an electric or magnetic field are shown by the black arrows, and the magnetoelectric coupling between the ferroelectric and ferromagnetic orders is shown by the green arrows.

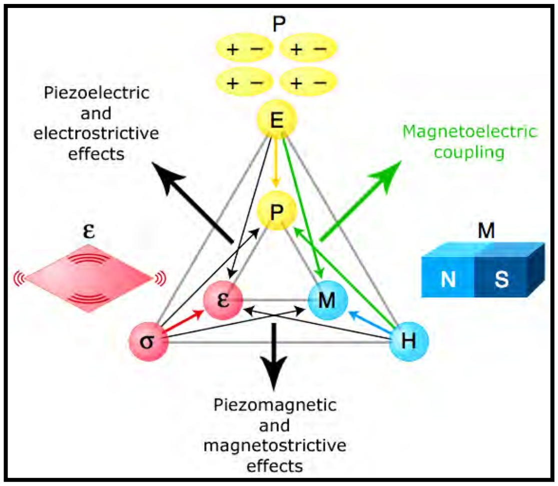

Figure 2.6: Ferroic orders and possible couplings between them.

2.4 Multiferroics and magnetoelectricity:

As the name suggests **multiferroic** are materials those posses more than one of the so called ferroic (ferroeletricity / ferromagnetism / ferroeleasticity) properties. In recent years this term is loosely used for the materials in which magnetism and ferroelectricity coexist. In 1894, P.Cuire [46] predicted that crystals could be simultaneously ferromagnetic and ferroelectric and magnetization in the crystal can be induced by the application of electric field and vice versa. This effect is known as "**magneto electric effect**" and the coupling between ferroelectric and magnetic interactions is known as "**magneto electric coupling**". It is clear from the definition of magneto electric coupling that the coexistence of ferroelectric and ferromagnetic orders is a necessary condition for the material to be classified as a magneto electric material; however, magneto electric coupling is an independent phenomenon that need not arise in all materials that are both magnetically and electrically polarizable. In practice, it is likely to arise in all materials that are both magnetically and electrically polarizable, either directly or via strain. This concept is pictorially depicted by several authors [1,47] through a schematic diagram as shown in Figure 2.7 In this diagram, ferromagnets (ferroelectrics) form a subset of magnetically (electrically) polarizable materials such as paramagnets and antiferromagnets (paraelectrics and antiferroelectrics) shown. The intersection of ferroelectric and ferromagnetic materials represents materials that are multiferroic and the smallest circle in the middle represents the materials that would show magneto electric coupling.

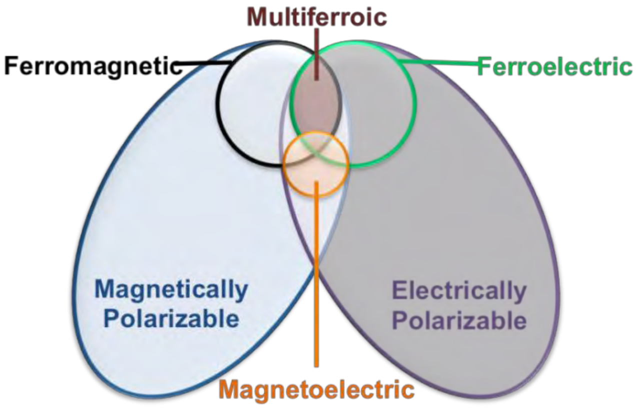

Figure 2.7 shows the intersection of two sets named magnetically and electrically polarizable material with subsets of ferromagnetic, ferroelectric, and intersection called multiferroic and magneto electric[46].

The materials which have coexistence of ferroelectric and magnetic orders and exhibit magneto electric coupling are called "**Magneto electric Multiferroics**".

2.5 Requirements for Magnetoelectric Multiferroics:

Although the experimental evidences of multiferroics and magnetoelectric phenomenon were started in the first half of 20th century, the numbers of the materials that exhibit magnetoelectric coupling were found to be rare. The coexistence of ferroelectric and magnetic orders itself is a challenging problem. In 2000, Hill discussed [48] in her review, the conditions required for ferroelectricity and ferromagnetism to be compatible in oxides; however, she also declared that these conditions are contradictory to each other and area difficult to be met in a material. The limiting factors which restrict the simultaneous existence of ferroelectricity and ferromagnetism are as given below.

2.5.1 Symmetry

The magnetoelectric effect was first predicted by P.Curie on the basis of symmetry considerations [46]. The primary conditions for ferroelectricity are the non-centrosymmetric structure, which allows the dipole formation and spontaneous polarization. There are 31 (out of 122) Shubnikov Heesch point groups that allow spontaneous electric polarization and 31 that allow spontaneous magnetization [49]. There is only 13 Shubnikov points, which allow both spontaneous magnetization and spontaneous electric polarization in same phase. The symmetry considerations itself restrict the number of multiferroics.

2.5.2 Electrons occupancy in d-orbital

In most of the perovskite multiferroics (ABO_3) the B-site is occupied by transition metals. According to electronic configuration, transition elements have empty, fully filled or partially filled d-orbitals that contribute to the electrical, magnetic and other physical properties of the material.

2.6 Types of Multiferroics

The microscopic origin of magnetism is basically the same in all magnets; it is the presence of localized electrons, mostly in the partially filled *d* or *f* shells of transition metal or rare earth ions, which have corresponding localized spin, or magnetic moment. Exchange interactions between localized moments lead to magnetic order. However the situation is different in case of ferroelectrics. There are several different microscopic origins of ferroelectricity and accordingly one can have different types of Multiferroics.

Generally the Multiferroics are categorized in two groups: (i) type I Multiferroics and (ii) type II Multiferroics, on the basis of the origin of ferroelectricity in them [1].

2.6.1 Type I Multiferroics

This group of Multiferroics contains those perovskites in which ferroelectricity and ferromagnetism have different sources (cations at A-site and B-site respectively). These materials show weak magnetoelectric coupling. In these materials, ferroelectricity typically appears at higher temperatures than magnetism and they exhibit large spontaneous polarization. Examples are BiFeO3 (T_c ~ 1110 K, T_N ~ 643 K, P ~ 90 μC/cm^2), $YMnO_3$ (T_c *FE* ~ 914 K, T_N ~ 76 K, P ~ 6 μC/cm^2). These materials have been extensively studied since 1960‟s. However, major challenge in these materials is to enhance the values of magnetoelectric coupling coefficient. Type I Multiferroics are further classified in many subclasses on the basis of origin of ferroelectricity.

(i)*Ferroelectricity due to shifting of B-cation*

Probably the best-known ferroelectrics are the perovskites like $BaTiO_3$ or $Pb(ZrTi)O_3$ (PZT). There are many magnetic materials among perovskites, and also many ferroelectrics. Theoretical studies have shown that the usual atomic-level mechanisms for ferromagnetism and ferroelectricity are quite different. Whereas for magnetism one needs partially filled d shells of a transition metal, practically all ferroelectric perovskites contain transition metal ions with an empty d shell, such as Ti^{4+}, Ta^{5+}, W^{6+}. Ferroelectricity in these systems is caused by the off-center shifts of the transition metal ion, which forms strong covalent bonds with one (or three) oxygens, using their empty d states. And somehow, the presence of real d electrons in d^n configurations of magnetic transition metals suppresses this process, preventing ferroelectricity in magnetic Perovskites. This so called "d^0 vs d^n problem" was one of the first to be studied theoretically at the beginning of the recent revival of multiferroics [50], and although there has been some progress, still there is no full solution of this problem [51]. The answer may well lie in the fact that this mutual exclusion is not a "theorem" but rather a matter of numbers: in most cases a magnetic d^n ion is stable in the center of its MO_6 octahedra, but there may still be the cases where it is not. One possible way around this problem may be making "mixed" perovskites with d^0 and d^n ions. However, the coupling of magnetic and ferroelectric subsystems in mixed perovskites is weak.

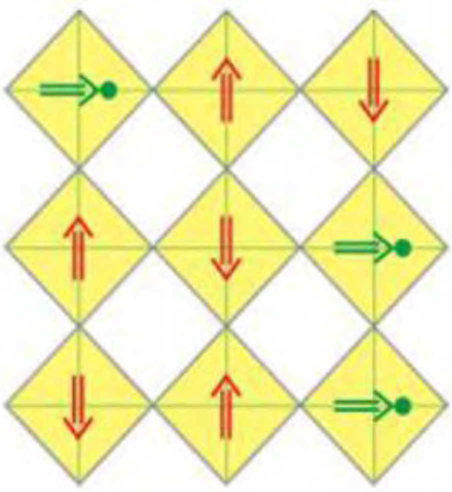

Figure 2.8: In "*mixed*" perovskites with ferroelectricity active d^0 ions (green circles) and magnetic d^n ions (red circles), shifts of d^0 ions from oxygen octahedral (yellow plaquettes) lead to polarization (green arrows), coexisting with magnetic order (red arrows).

(ii) *Ferroelectricity due to lone pairs*

These multiferroic materials exhibit ferroelectricity due to lone pair at A-site cation. Most of Bismuth (Bi) and Lead (Pb) based perovskites show ferroelectricity *due to lone pair*, for example $BiFeO_3$, $BiMnO_3$, and $PbVO_3$. In these materials Bi^{3+} and Pb^{2+} have two outer 6*s* electrons that do not participate in chemical bonds. These electrons are called "*lone pairs*" or sometimes dangling bonds. Microscopically, one can explain the origin of ferroelectricity in these compounds by the ordering of these lone pairs (with certain admixture of *p*-orbitals) in the direction of electric field. The magnetism in these materials is originated from B-cation.

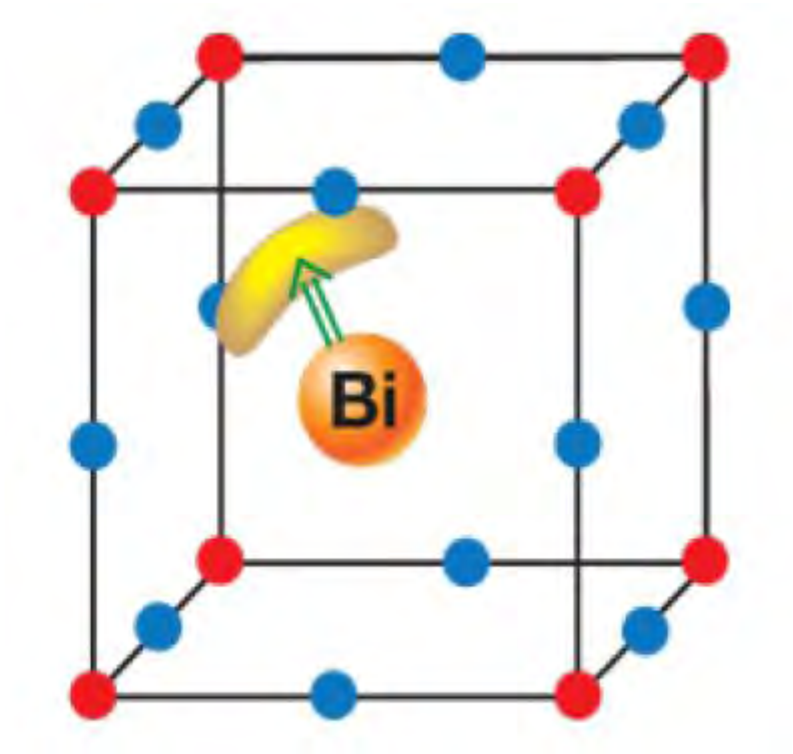

Figure 2.9: In materials like $BiFeO_3$ and $PbVO_3$, the ordering of lone pairs (yellow "lobes") of Bi^{3+} and Pb^{2+} ions (orange), contributes to the polarization (green arrow) [52].

(iii) *Ferroelectricity due to charge ordering*

This is another group of ferroelectrics, in which the electric polarization is induced *due to the non-centrosymmetry of charges*. The non-centrosymmetry of charges is normally observed in transition metal compounds (especially transition metal ions with different metal states) e.g. $Pr0.5Ca0.5MnO_3$ or in Nickelates $RNiO_3$ [48].

(iv) *"Geometric" ferroelectricity*

In this category of Multiferroics, some geometric disorder in the lattice causes ferroelectricity. For example in case of $YMnO_3$, ferroelectricity has nothing to do with individual cations, but is caused by the tilting of practically rigid MnO_5 block with respect to Y-ions [48]. This tilting occurs just to provide closer packing, and as a result the oxygen ions moves closer to the rather small Y ions.

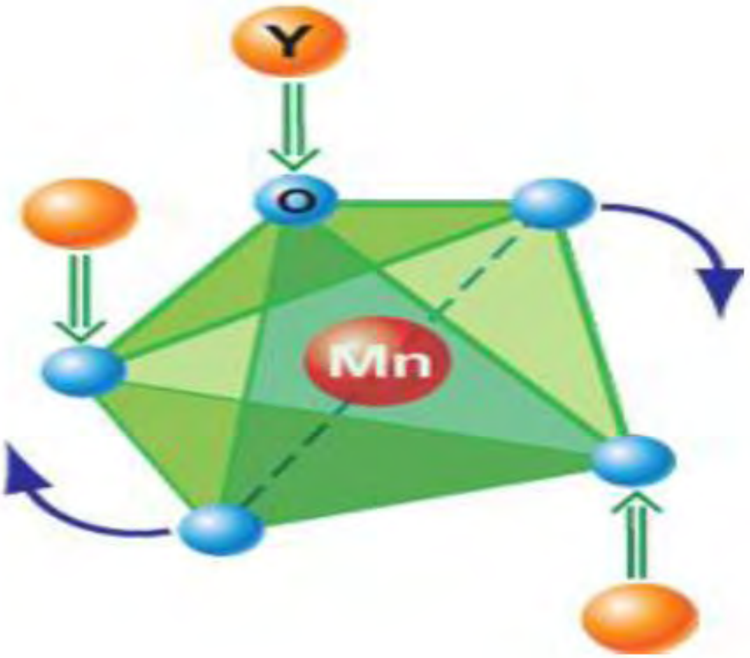

Figure 2.10: The "geometric" mechanism of generation of polarization in YMnO3 [48] describes the tilting of a rigid MnO5 block with a magnetic Mn remaining at the center. Because of the tilting, the Y-O bonds form dipoles (green arrows), and there appears two"up" dipoles per one "down" dipole so that the system becomes ferroelectric (and multiferroic when Mn spins order at lower temperatures).

2.6.2 Type II Multiferroics (Magnetic Multiferroics)

The materials in which the ferroelectricity is originated from magnetism and implies strong magnetoelectric coupling. However the polarization in these materials is usually much smaller (10^{-2} μC/cm2). These Multiferroics are recently discovered. $TbMnO_3$ and $TbMn_2O_5$ are typical examples of these materials [53,54]. Kimura *et al* [53] demonstrate strong influence of magnetic field on electric polarization. In TbMnO3, the polarization rotates (or "flops") by 90 degrees when a critical field is applied in a certain direction [53]. Influence of magnetic field is even stronger in case of $TbMn_2O_5$ [54]. The polarization changes sign with magnetic field. Since the discovery of these materials, a number of other type-II Multiferroics with strong magnetoelectric coupling have been discovered and studied. On the basis of mechanism of multiferroic behavior, one can divide type-II Multiferroics in two categories.

(i)*Spiral Type-II Multiferroics*

In this type of Multiferroics, the ferroelectricity appears in conjunction with a spiraling magnetic phase, mostly cycloid type. $TbMnO_3$, $Ni_3V_2O_6$ and $MnWO_4$ are typical examples of this type of multiferroics. Therefore, these type-II multiferroics are usually found in frustrated magnetic systems.

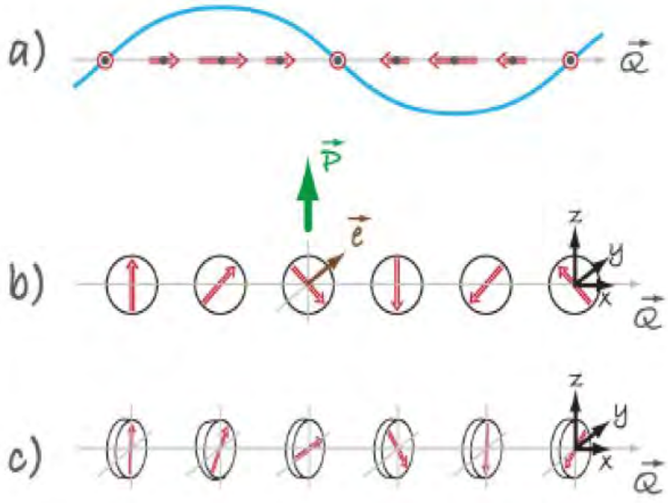

Figure 2.11: Different types of spin structures relevant for type-II Multiferroics (a) Sinusoidal spin density wave, in which spins point along one direction but vary in magnitude. This structure is centrosymmetic and consequently not ferroelectric. (b) The cycloidal spiral with the wave vector **Q** = Qx and spins rotating in the (x,z)-plane. It is in this case where one finds nonzero polarization, $P_z \neq 0$. (c) In a so-called "proper screw" the spins rotate in a plane perpendicular to **Q**. Here the inversion symmetry is broken, but most often it does not produce polarization, although in certain cases it might [55].

(ii) *Type-II Multiferroics with Collinear Magnetic Structures*

In this group of Type-II multiferroics ferroelectricity appears in collinear magnetic structures; *i.e.,* all magnetic moments are aligned along a particular axis without the necessary involvement of spin-orbit interaction. Polarization can appear in these materials as a consequence of exchange striction because the magnetic coupling varies with atomic positions. The simplest example of this type of multiferroics is Ca_3CoMnO_6 [56].

2.6.3 Multiphase multiferroics

The choice of single-phase materials exhibiting the coexistence of at least two ferroic orders at room temperature is quite limited. The scarcity of single phase multiferroic materials makes composite/ multiphase multiferroics an interesting alternative. Magnetoelectric multiferroic composites consist of a ferroelectric phase and ferromagnetic phase, and the coupling between the two orderings is through stress mediation. The magnetoelectric effect is extrinsic in this case since magnetoelectric effect is not exhibited by any of the constituent phases on their own. Various constituent materials have been studied as multiferroic composite materials, such as $BaTiO_3$-$CoFe_2O_4$, $BaTiO_3$-$NiFe_2O_4$, PZT-$NiFe_2O_4$, PZT-$CoFe_2O_4$, $BiFeO_3$-$CoFe_2O_4$, and $BiFeO_3$-$NiFe_2O_4$.

2.7 Bismuth Ferrite ($BiFeO_3$)

Bi-based compounds are of main interest due to their multiferroic behavior. There are many Bi-based perovskite compounds in which B-site is accommodated by transition metals e.g. BiFeO3, BiMnO3, BiCrO3 etc. These compounds fall into the category of "**type-I multiferroics**". Ferroelectricity originates from the alignment of lone pair of Bi3+ ion and magnetism comes from B-site atom (Mn or Fe).

$BiFeO_3$ is one of the most extensively studied multiferroic material in recent years and it is the only material known to exhibit magnetic order (T_N= 643 K) and ferroelectric order (ferroelectric transition temperature T_c FE= 1103 K) at room temperature. The properties of the material are discussed in this section [57].

2.7.1 Structure

Single crystal $BiFeO_3$ owns a rhombohedrally distorted perovskite structure belonging to the space group of $R3c$ with a lattice parameter of a = 5.62 Å and α = 59.35° [3]. Meanwhile, the structure of $BiFeO_3$ could also be characterized by two distorted perovskite unit cells (ar = 3.96 Å, αr = 89.3~89.4°) connected along their body diagonal, denoted by the pseudocubic <111>, to form a rhombohedral unit cell [51]. The Fe-O-Fe angle is important since it dominates both the magnetic exchange and orbital overlap between Fe and O, and as such it controls the magnetic ordering temperature and the conductivity [52]. One of the Bi-Fe distances also has a local maximum near Néel temperature, and the atomic vibrations of Bi^{3+} and O^{2}- ions show a significant anisotropy [52].

The ferroelectric state arises from a large displacement of the Bi ions relative to the FeO_6 octahedra. The ferroelectric polarization lies along the pseudocubic <111> leading to the formation of eight possible polarization variants, corresponding to four structural variants [48]. The antiferromagnetic ordering of $BiFeO_3$ is G-type, in which the Fe magnetic moments are aligned ferromagnetically within (111) and antiferromagnetically between adjacent (111) [51]. In addition, $BiFeO_3$ exhibits a spin cycloid structure in the bulk [10] while the preferred orientation of the antiferromagnetically aligned spins is in the (111), perpendicular to the ferroelectric polarization direction with six equivalent easy axes within that plane (Figure 2.12). $BiFeO_3$ thin films have shown the existence of a large ferroelectric polarization as well as a small net magnetization of the Dzyaloshinskii–Moriya type resulting from a canting of the antiferromagnetic sublattices [11].

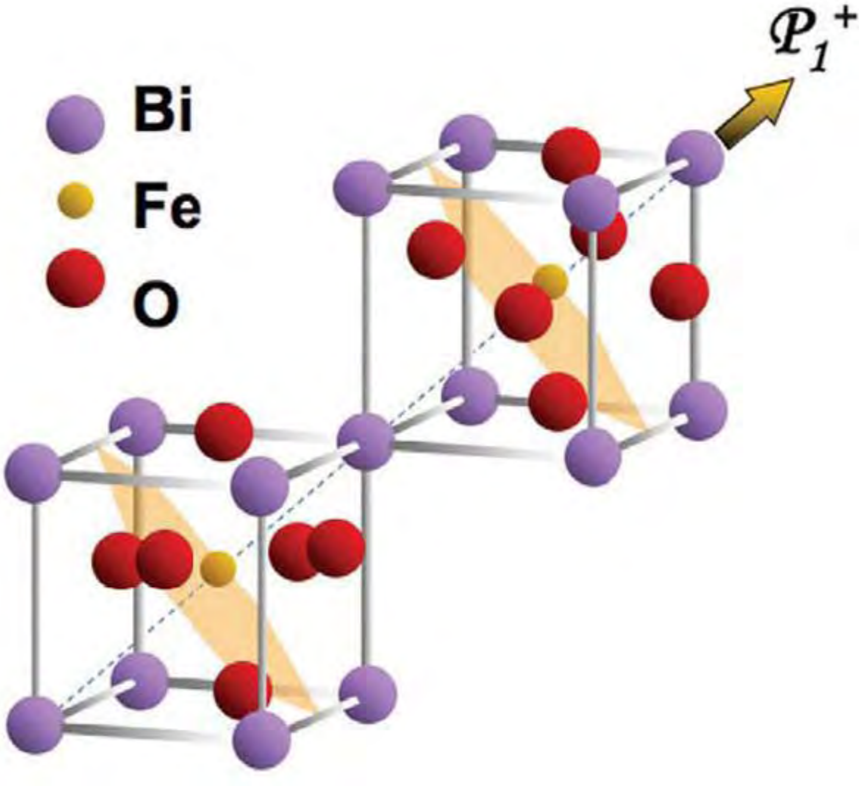

Figure 2.12: Schematic of crystal structure of BFO and ferroelectric polarization (arrow) and antiferromagnetic plane (shaded planes) .

The ferroelectric state arises from a large displacement of the Bi ions (A-site polarization) relative to the FeO_6 octahedra in $BiFeO_3$ as shown in Figure 2.13. The ferroelectric polarization lies along the pseudocubic <111> leading to the formation of eight possible polarization variantsts.

Whether A-site and B-site polarization occurs depends on Goldschmid Tolerance Factor, $t = (r_{A\text{-site}}+r_O)/\sqrt{2}(r_{B\text{-site}}+r_O)$;

If t<1 the oxygen octahedra must buckle in order to fit into a cell that is too small.

For, $BaTiO_3$, $t=(1.5+1.28)/\sqrt{2}(0.75+1.28)=.98\sim1$; **Slight or no buckle** (B-site polarization)
For, $BiFeO_3$, $t=(1.17+1.28)/\sqrt{2}(0.69+1.28)=.88$; **Buckling Occurs** (A-site polarization)

This buckling of FeO_6 octahedra in $BiFeO_3$ is the main cause behind A-site polarization.

The displacement of the A-site bismuth cation (shown in Figure 2.12) along the [111] axis due to octahedra buckling brings about a non-centrosymmetric polarization resulting in the ferroelectric property.

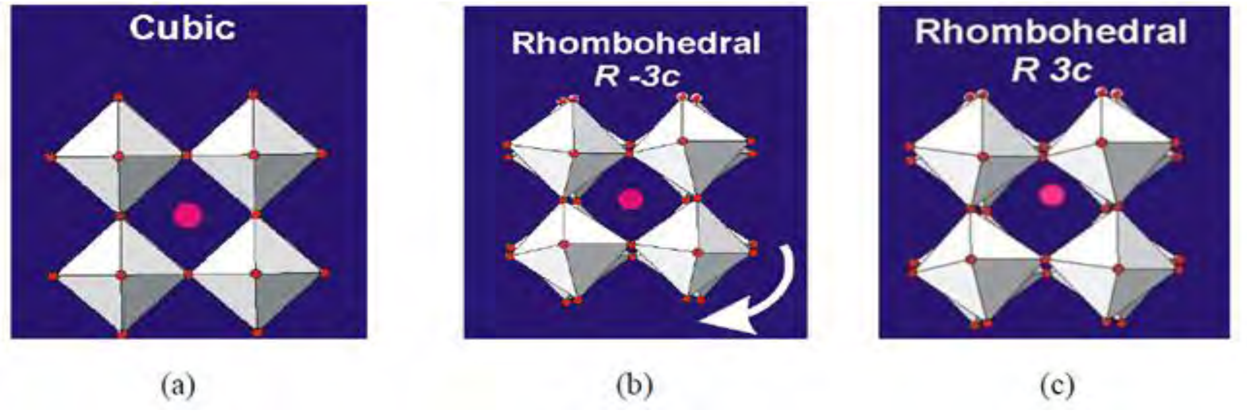

Figure 2.13: Schematic illustration of a structural transition process.[(a) ideal cubic structure Pm-3m without tilting; (b) R-3c structure tilted along three axes with the same angle; (c) Displacement of Bi ion towards [111] direction based on R-3c.]

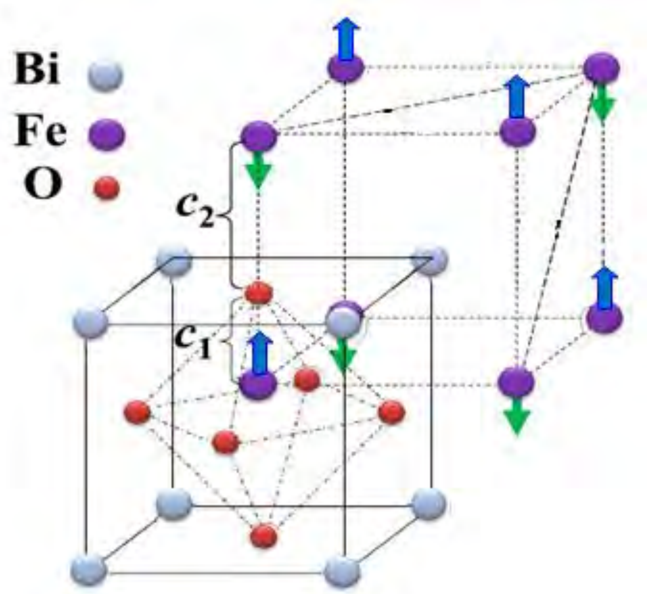

Figure 2.14: (Colour on-line) Schematic of tetragonal-like $BiFeO_3$ (BFO) with G-type antiferromagnetic ordering.

magnetic ordering of $BiFeO_3$ is G-type antiferromanget: each Fe^{3+} spin is surround by six nearly antiparallel spins on the nearest Fe neighbours (Figure 2.14). The antiferromagnetic spin ordering is not homogeneous but is manifested as an incommensurated cycloid structure with a wavelength of ~ 64 nm along <110>, as can be seen in Figure 2.15 [38]. In this cycloid structure the net magnetic moment of the spins cancel out each other and results in zero net magnetization. The spin rotation plane can also be determined because the magnetic scattering amplitude depends on the component of magnetic moments perpendicular to the scattering vector. The magnetic Néel temperature is about 643 K and the cycloid could be distorted at low temperatures [12].

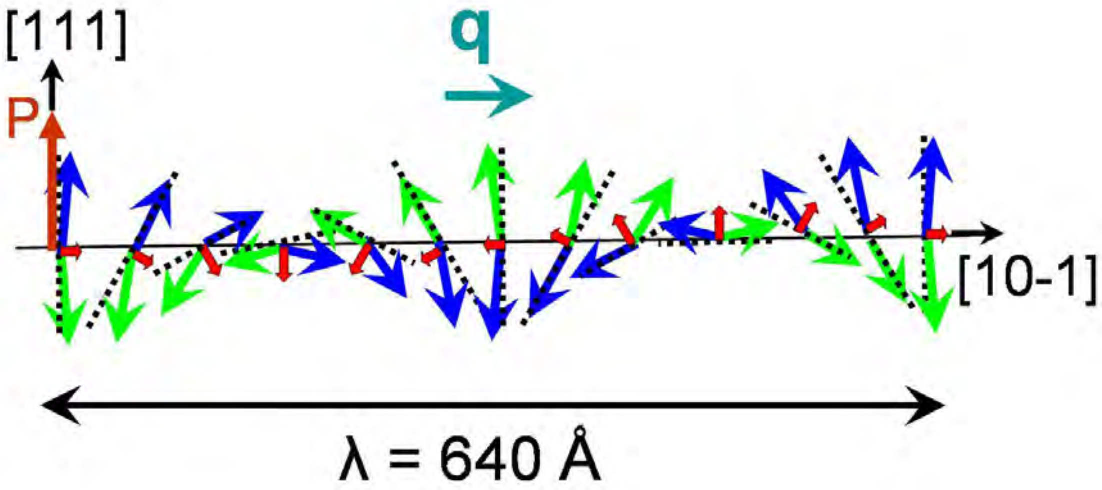

Figure 2.15: Schematics of the 64 nm antiferromagnetic circular cycloid. [The canted antiferromagnetic spins (blue and green arrows) give rise to a net magnetic moment (purple arrows) that is specially averaged out to zero due to the cycloidal rotation. The spins are contained within the plane defined by the polarization vector [38].]

2.7.2 Synthesis and Phase Diagram of $BiFeO_3$

$BiFeO_3$ is a typical multiferroic material that has been extensively investigated nowadays. The initial research on $BiFeO_3$ was carried out by Smolenskii in1960 [58]. But at that time, they were not able to make single-phase polycrystalline$BiFeO_3$ and the $BiFeO_3$ produced was not stable for practical application. In 1967, Achenbach successfully prepared single-phase $BiFeO_3$ by removing the undesirable phases using HNO_3 [59]. X-ray diffraction technique was also adopted to investigate the monodomain single-phase by Kubel and Schmid in 1990 [6]. Later in 2003, Ramesh and his colleagues produced thin film $BiFeO_3$ which exhibited remnant polarization 15 times stronger than that of the bulk $BiFeO_3$ [20]. Until recently, increasing efforts have also been devoted to the research focusing on the preparation and characterization of $BiFeO_3$ in forms of film, bulk and nanostructure.

However, single phase BiFeO3 is difficult to synthesize. Due to the metastable nature of bismuth ferrite in air 20 as well as the volatility of bismuth oxide, their stoichiometry can be changed resulting in impurities of Bi_2O_3, $Bi_{25}FeO_{39}$ and Bi_2FeO_9 during the sintering process. The phase diagram of Fe_2O_3 and Bi_2O_3 is presented below in Figure 2.16 [60], unequal amount of Fe_2O_3 and Bi_2O_3 is seen to bring about impurity phases $Bi_{25}FeO_{39}$ (bismuth-rich) and Bi_2FeO_9 (bismuth-deficient).

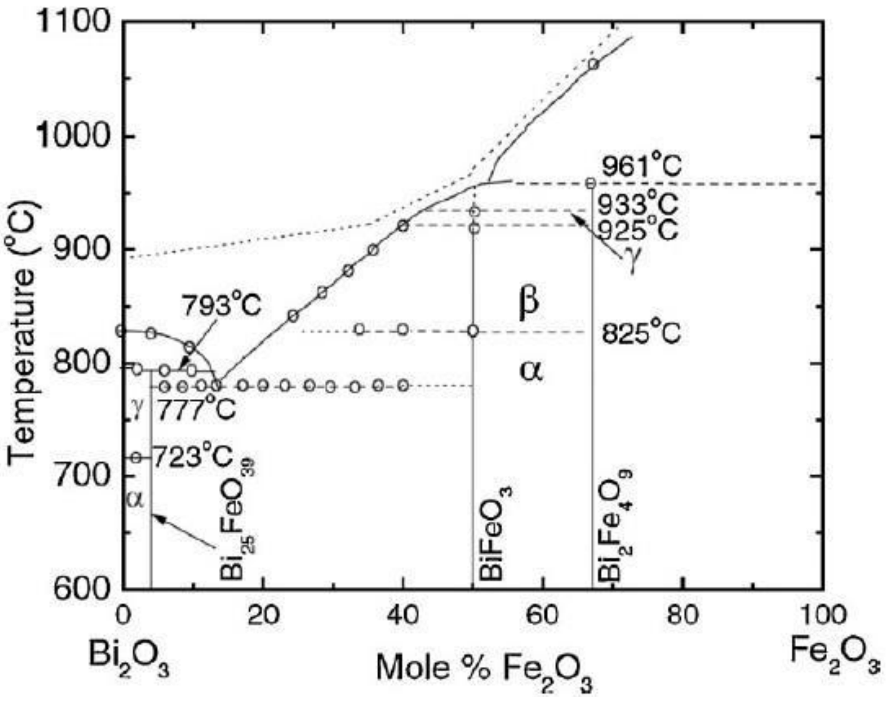

Figure 2.16: Phase diagram of Fe2O3and Bi2O3showing bismuth ferrite with undesired impurities [60].

CHAPTER 3

EXPERIMENTAL

3.1 Introduction

Among the various wet chemical processes, the pechini sol-gel route is found to be simple and cost effective for the synthesis of homogeneous and very fine crystalline nanopowders. The process is based on the mixing of reactants that oxidize easily, such as metal nitrates, and an organic chelating agent that acts as reducing agent.

The various advantages of sol-gel synthesis as the prime method for the production of $BiFeO_3$ are

- Self-purification due to the high exothermic temperatures involvement.
- Formation of nano- powders in the desired size and shape with uniform particle size distribution.
- Simple and cost effective.
- Synthesis of single phase materials at very low temperatures.

3.2 Synthesis Procedure

Bismuth ferrite was prepared by a modified pechini sol-gel method using Citric acid as the chelating agent. The reagents used in the present work were analytical grade bismuth nitrate pentahydrate ($Bi(NO_3)_3 \cdot 5H_2O$), iron nitrate nonahydrate ($Fe(NO_3)_3 \cdot 9H_2O$), citric acid ($C_6H_8O_7$), ethylene glycol ($C_2H_6O_2$) and glacial acetic acid (CH_3COOH).

- Stoichiometric proportion of $Bi(NO_3)_3.5H_2O$ and $Fe(NO_3)_3.9H_2O$ were initially dissolved in 400 ml deionized water with an individual concentration of 0.025M.
- The solution was stirred for about half an hour to obtain a clear solution.
- When the solution was transparent, 0.02 mole of $C_6H_8O_7$ as the chelating agent was added to the solution to complex the metal cations (Figure 3.1a).
- The solution was then stirred and heated at 70-75°C for 8-10 hrs to form a transparent blackish-red sol (Figure 3.1b).
- pH of the solution was maintained between 1-2 all-time by adding NH_4OH dropwise.

- Afterwards appropriate amount of ethylene glycol was added to the solution as polymerization agent.
- The resultant solution was heated at 85-90°C to initiate the polymerization reaction and a few minutes later a gel was formed with vigorous boiling and fuming (Figure 3.1c).
- The gel was dried at 100°C for 24 hrs in a drier to obtain fluffy green xerogel (Figure 3.1d).
- The same procedure was repeated to produce xerogel for annealing at different temperatures.
- The xerogel samples were then ground into powders and annealed at 400-600°C for 2 hrs in static air to get $BiFeO_3$ nanoparticles (Figure 3.1f).
- Another xerogel sample was also annealed at temperature as high as 800°C to obtain bulk $BiFeO_3$ sample.
- The heating and cooling rate of the furnace were maintained at 3°C/min.
- The powders thus obtained were washed with CH_3COOH followed by deionized water at 70 °C to remove impurity phases from $BiFeO_3$.
- Finally the powders were dried for characterization.

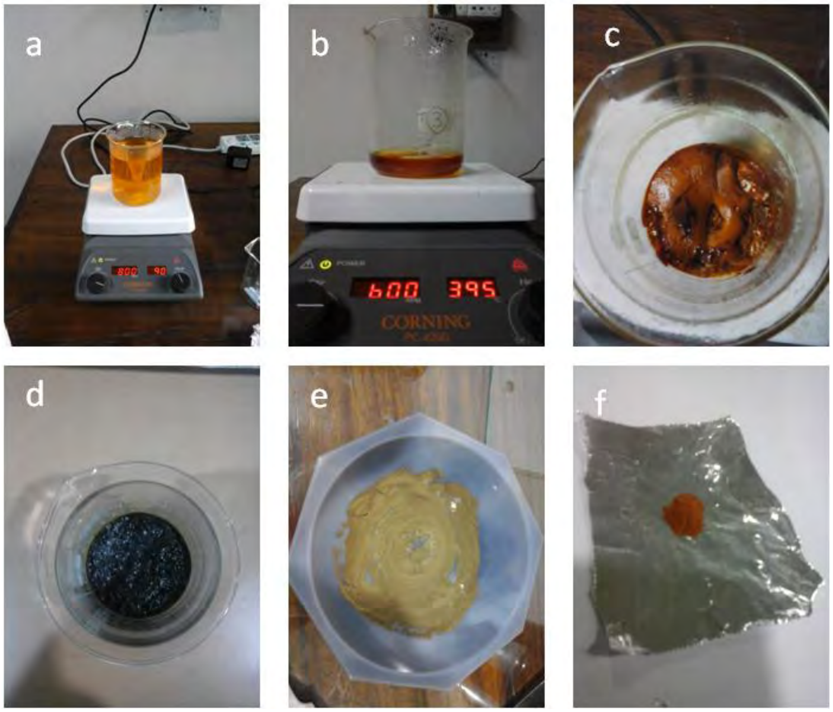

Figure 3.1: Synthesis steps a) mixing raw materials into deionized water, b) formation of sol, c) formation of gel, d) precursor xerogel e) ground xerogel, f) annealed $BiFeO_3$ powder.

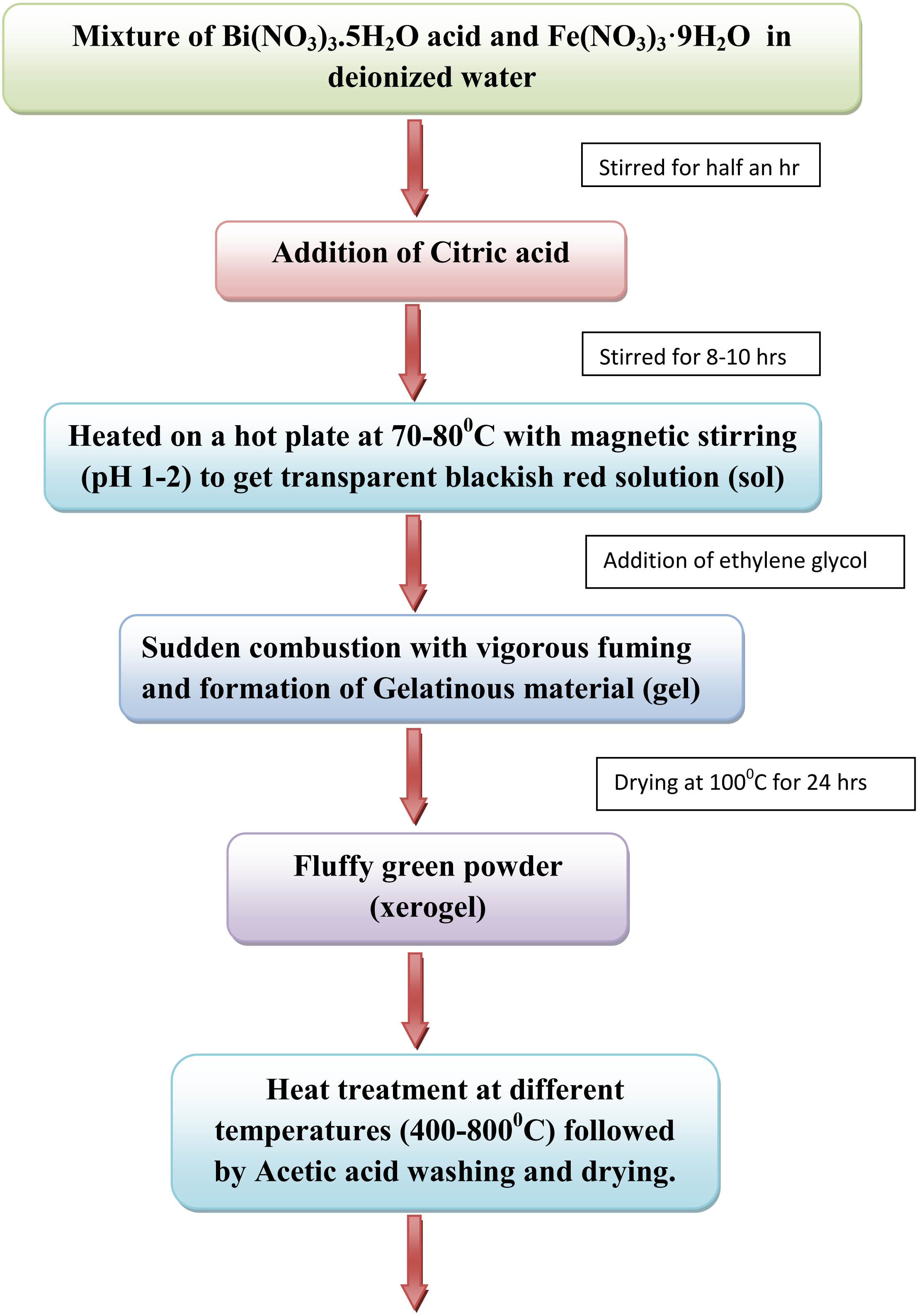

Characterization of the obtained $BiFeO_3$ nanoparticles

3.3 Annealing

Flow chart for $BiFeO_3$ powder synthesis

Muffle Furnace (Nabertherm GmbH Bahnhofstr, 20, Lilienthal / Bremen Germany) was used to anneal xerogel samples at 400^0C, 450^0C, 500^0C, 550^0C, 600^0C and 800^0C in air atmosphere. The basic annealing cycle in this experiment is shown in Figure 3.3

Figure 3.2: Furnace used for annealing xerogel sample.

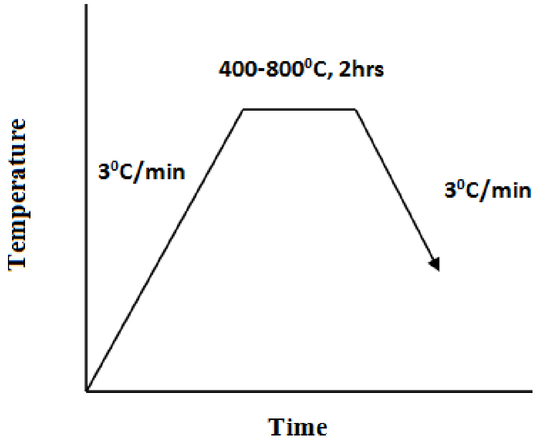

Figure 3.3: Annealing cycle

3.4 Thermogravimetric analysis

Thermo gravimetric (TG) analysis (model Q 50, TA Instruments) was carried out to investigate the decomposition and pyrolysis of the $BiFeO_3$ precursor xerogel up to 600^0C at a heating rate of 10°C/min in static air.

Figure 3.4: Thermogravimetric analyser.

Thermogravimetric analysis or thermal gravimetric analysis (TGA) is a method of thermal analysis in which changes in physical and chemical properties of materials are measured as a function of increasing temperature. TGA is commonly used to determine selected characteristics of materials that exhibit either mass loss or gain due to decomposition, oxidation, or loss of volatiles (such as moisture). Common applications of TGA are (1) materials characterization through analysis of characteristic decomposition patterns, (2) studies of degradation mechanisms and reaction kinetics, (3) determination of organic content in a sample, and (4) determination of inorganic (e.g. ash) content in a sample, which may be useful for corroborating predicted material structures or simply used as a chemical analysis.

3.5 Fourier transform infrared spectroscopy

Fourier transform infrared spectroscopy, FTIR (model Nicolet 380, Thermo Scientific) was used to determine the chemical bonding of the $BiFeO_3$ precursor xerogel and annealed powders.

Figure 3.5: Fourier transform infrared spectrometer

About 1-2% of the sample was mixed and ground with KBr to a fine powder. Although a homogeneous mixture gives the best results, excessive grinding of the potassium bromide is not required. Two stainless steel disks and a die were taken from the desiccators. Finely ground mixture was filled in the die between the two steel disks. Then two tons of loads were applied on the sandwich disks to form pallet. Then the pallet was placed inside the FTIR sample holder to carry out the test.

3.6 Field Emission Scanning Electron Microscopy

To observe morphology of the synthesized powders we used field emission scanning electron microscope, FESEM (JEOL JSM 7600F). Powder samples were adhered with carbon tape that was attached to a Copper stub. Samples were made conductive, coated with platinum by ion sputtering method. Then sample holder was mounted on a holder and inserted in FESEM. The micrographs obtained from FESEM analysis was used for microstructural study.

Figure 3.5: Field Emission Scanning Electron Microscope (FESEM).

3.7 X-Ray Diffraction Study

X-ray diffraction analysis was conducted using the XRD (3040-X"Pert PRO, Philips) facility in order to determine the phases present in the synthesized powers. The high-intensity CuKα radiation was focused on the sample in the scanning range from 10° to 70°.

Figure 3.6: XRD Machine.

X-rays are a type of electromagnetic radiation. The wavelength of x-rays is approximately 1 Å which has the same size equivalent to that of an atom. X-ray diffraction (XRD) is a non-destructive analytical technique mainly used for the phase identification and structural characterization of crystalline materials.

The relationship between the wavelengths of the X-rays λ, the incidence angle θ, and spacing between two crystal lattice planes (hkl) d, is shown in the Bragg's Law expressed as:

$$2d_{hkl} \sin\theta = n\lambda \quad (3.1)$$

After characterization by X-ray diffraction, a number of peaks are seen in the diffraction patterns. These patterns are identified by comparing their positions and relative intensities with the known structures in the database. Sometimes extra peaks might appear due to the impurity or structural transformation after thermal treatment. In fact, the intensity, width and position of peaks in the patterns reflect information about structure, quantity, texture etc. of crystallites.

The average crystallite size (*d*) of the synthesized powders was calculated from the XRD patterns using the Scherrer formula,

$$d = k\lambda/\beta\cos\theta \quad (3.2)$$

where k is the dimensionless shape factor with a typical value of about 0.9, λ is the wavelength of Cu Kα radiation with the value of 1.5418 Å, θ is the Bragg angle for the diffraction peak and β is the full width at half maximum intensity (FWHM) of the corresponding diffraction peak.

3.8 Vibrating sample magnetometer

A vibrating sample magnetometer, VSM was used to determine the magnetic properties of the synthesized powders at three different temperatures (80k, 200K, 300K) up to applied field of 16.5 kOe. The principle of this measurement is as follows: when a sample is placed in a homogeneous magnetic field, a magnetic moment is induced in the sample. If this sample is made to undergo sinusoidal motion, the vibration induces a magnetic flux change. This in turn induces a voltage in the pick-up coils. The magnetic moment determined by the VSM is related to the magnetization of the sample and its susceptibility. In this study, the magnetic property was characterized using a Lakeshore 7407 vibrating sample magnetometer (VSM). The sample was suspended from a vibrating drive head by a non-magnetic rod and placed between two electromagnets which produce a magnetic field. The vibrator generated a vertical sinusoidal vibration, thus the sample experiences sinusoidal motion, inducing an electrical signal in the coils mounted on the pole faces to the electromagnets. The signal picked up by the coils is proportional to the frequency and amplitude of the sinusoidal motion, and the total magnetic moment of the sample at the applied magnetic field. The frequency and amplitude of the sinusoidal were maintained constant by a capacitor. By feeding the signal from the pick-up coils and the reference signal into a demodulator, the magnetic moment of the sample was extracted.

Figure 3.7: Vibrating Sample Magnetometer.

CHAPTER 4
RESULTS AND DISCUSSION

4.1 Introduction

Very low magnetic moment is one of the mostly reported weaknesses which have stymied the potential applications of $BiFeO_3$ [37]. G type antiferromagnetism with a spiral spin structure having a period of 62 nm subdues any net magnetization in bulk $BiFeO_3$.Therefore, much work have been done to improve the magnetic properties of $BiFeO_3$. A number of studies have shown that doping with rare-earth, alkaline-earth and transition elements modify the spiral spin structure of $BiFeO_3$ and hence improve magnetization [8, 13 and 31]. On the other hand, recently enhanced magnetization in $BiFeO_3$ nanoparticles and thin films has received a great attention. If the characteristic length of nanoparticles or thin film is less than 62 nm, the spiral spin structure is suppressed resulting in net magnetization value [35]. This was the motivation for synthesis and investigation of magnetic properties of $BiFeO_3$ nanoparticles. But synthesis of pure and very uniformly distributed particles is really difficult. In the present work, a systematic study is reported on the effect of particle size on structural and magnetic properties of $BiFeO_3$ nanoparticles synthesized by modified pechini sol gel method.

4.2 Optimizing synthesis parameter:

As stated in section 1.4, one of the aims of this thesis is to synthesize nanocrystalline $BiFeO_3$ with uniform and homogenous particle size distribution at low temperature. At the very beginning conventional pechini sol-gel route was adopted to synthesize $BiFeO_3$ nanoparticles using citric acid as a chelating agent. The advantages of using citric acid include low decomposition temperature and synthesis of materials with homogeneous microstructure.

$BiFeO_3$ powder was prepared by adopting the synthesis technique as described in the section 3.2. Initially for test 1, conventional pechini sol-gel route was adopted to synthesize bismuth ferrite nanoparticles. No polymerization agent or surfactant except citric acid was used. The adopted synthesis conditions for different tests are mentioned in table 4.1.

Table 4.1: Different test conditions for $BiFeO_3$ synthesis.

Test no	Concentration of $Fe(NO_3)_3.\ 9H_2O$	Concentration of $Bi(NO_3)_3.\ 5H_2O$	Concentration of Citric acid	Concentration of Ethylene Glycol
Test 1	0.0125	0.0125	0.025	0
Test 2	0.0125	0.0125	0.025	0.0125
Test 3	0.0125	0.0125	0.025	0.025
Test 4	0.0125	0.0125	0.025	0.050

For test 1 $BiFeO_3$ powder was synthesized without using ethylene glycol as surfactant agent. At that instant the precursor xerogel was annealed at 400^0C. The microstructure of the synthesized powders for test 1 is depicted in Figure 4.1.

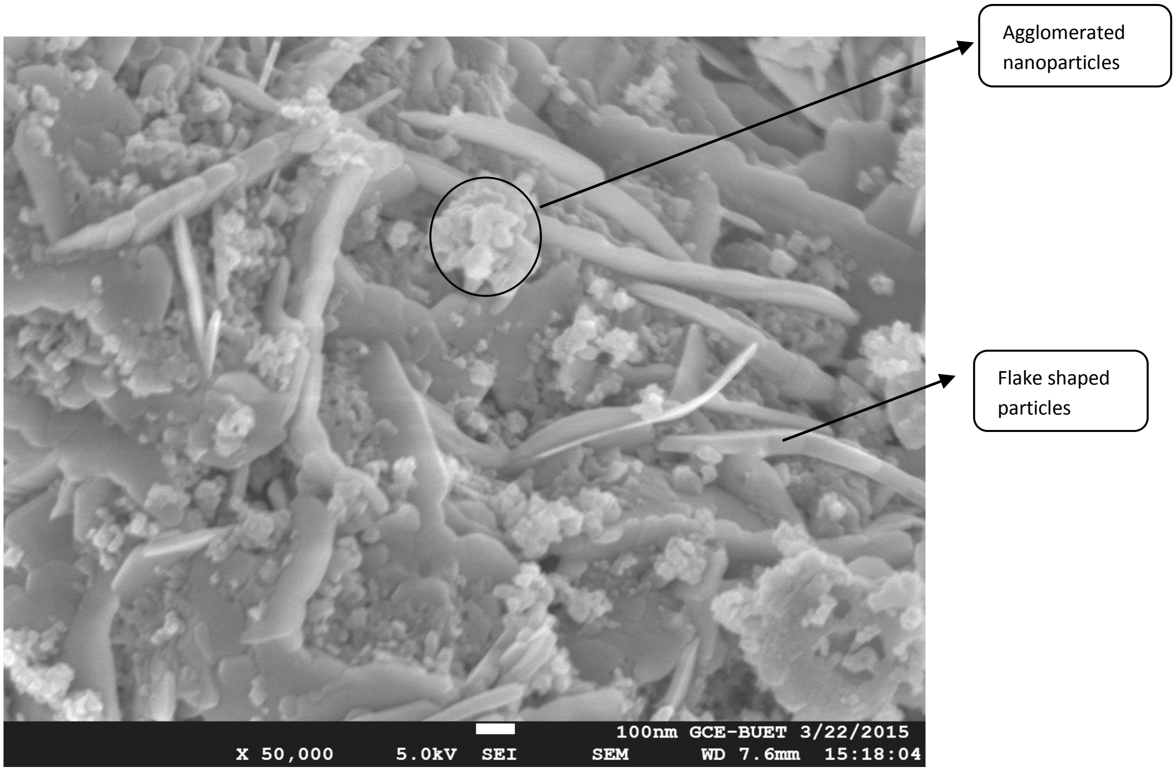

Figure 4.1: FESEM micrograph of $BiFeO_3$ powders annealed at 400^oC for 2 hour (Test 1).

XRD analysis confirmed that the synthesized material was $BiFeO_3$ (Figure 4.2). Though there are some particles in the microstructure, the morphology of the synthesized material was quite different from the targeted shape and size distribution. The rod and flake shape structure in the FESEM micrograph clearly demonstrated the lack of surfactant action during synthesis.

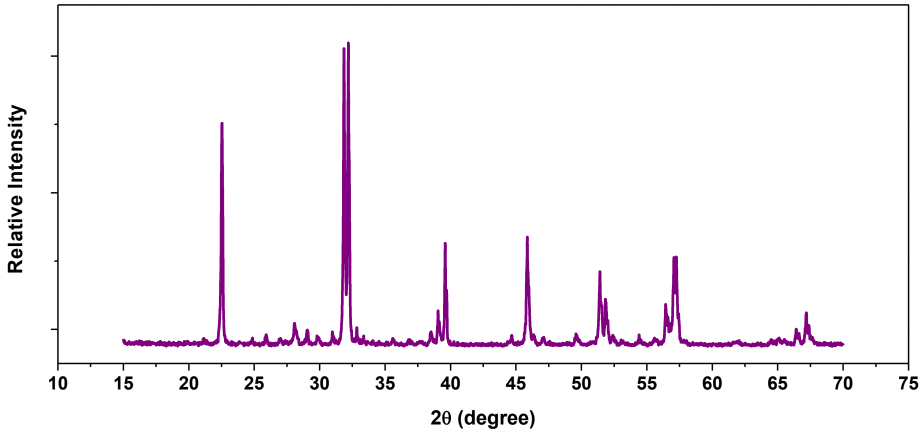

Figure 4.2: X-ray diffraction pattern of $BiFeO_3$ particles annealed at 400^0C (Test 1)

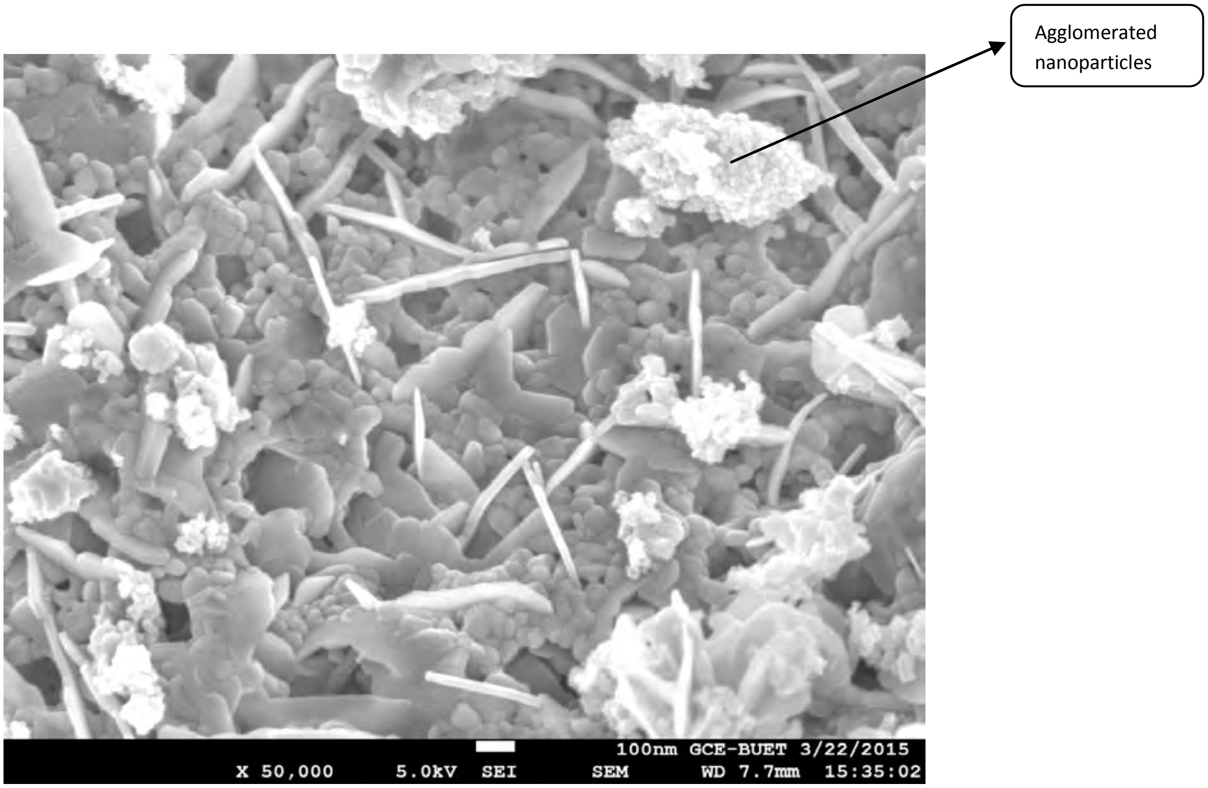

Figure 4.3: FESEM micrograph of $BiFeO_3$ powders annealed at 400^oC for 2 hour (Test 2).

Several attempts to modifty conventional pechini method have been reported in literature to improve morphology of the synthesized powder. Glucose, PVA, acetic acid and ethylene glycol could be a successful addition as surfactant agent. In this study ethylene glycol was chosen as a polymerization and surfactant agent. Ethylene glycol with concentration 0.0125 M was used in test 2 and the morphology of the synthesized powders are shown in Figure 4.3.

The surfactant action of ethylene glycol is vivid in the FESEM micrograph. Many nanocrystalline particles appeared in the microstructure. But still there were considerable flake shaped particles. So the concentration of ethylene glycol was increased in test 3 and continued the same procedure of synthesis to observe the nature of microstructure.

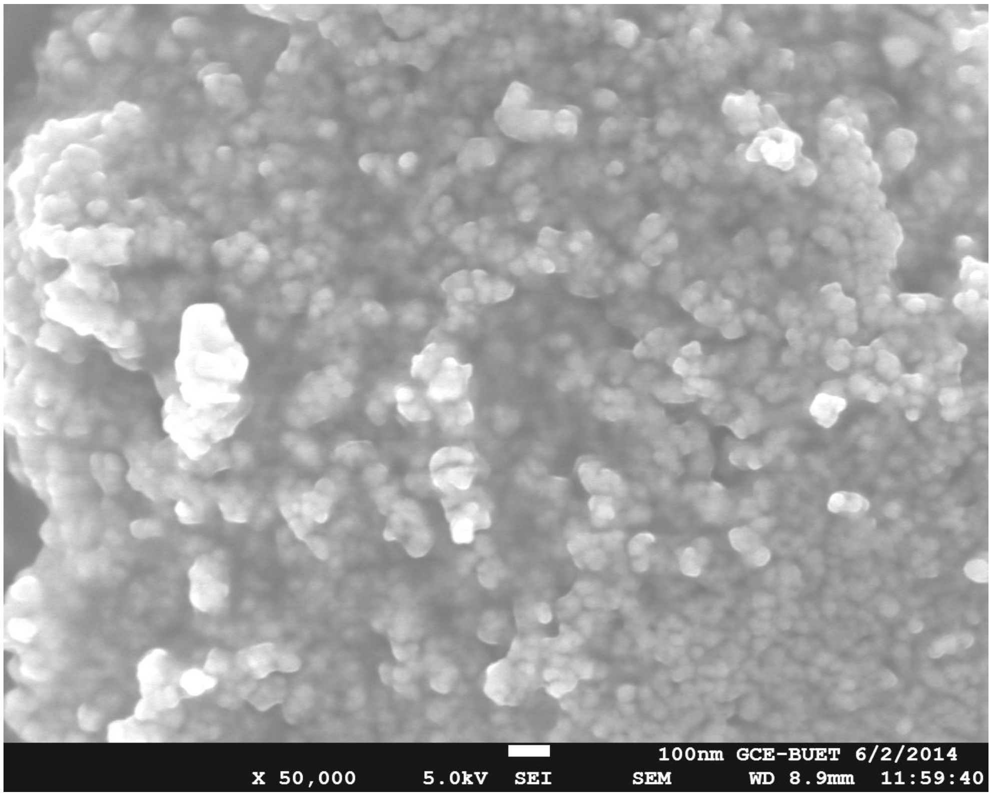

Figure 4.4: FESEM micrograph of $BiFeO_3$ powders annealed at 400^oC for 2 hour (Test 3).

Very fine nanocrystallites appeared in the FESEM micrograph for test 3 (Figure 4.4). Though the particles are very fine and uniform, the agglomerated condition of the synthesized powders encouraged us for further addition of ethylene glycol in test 4 to attain expected microstructure modification.

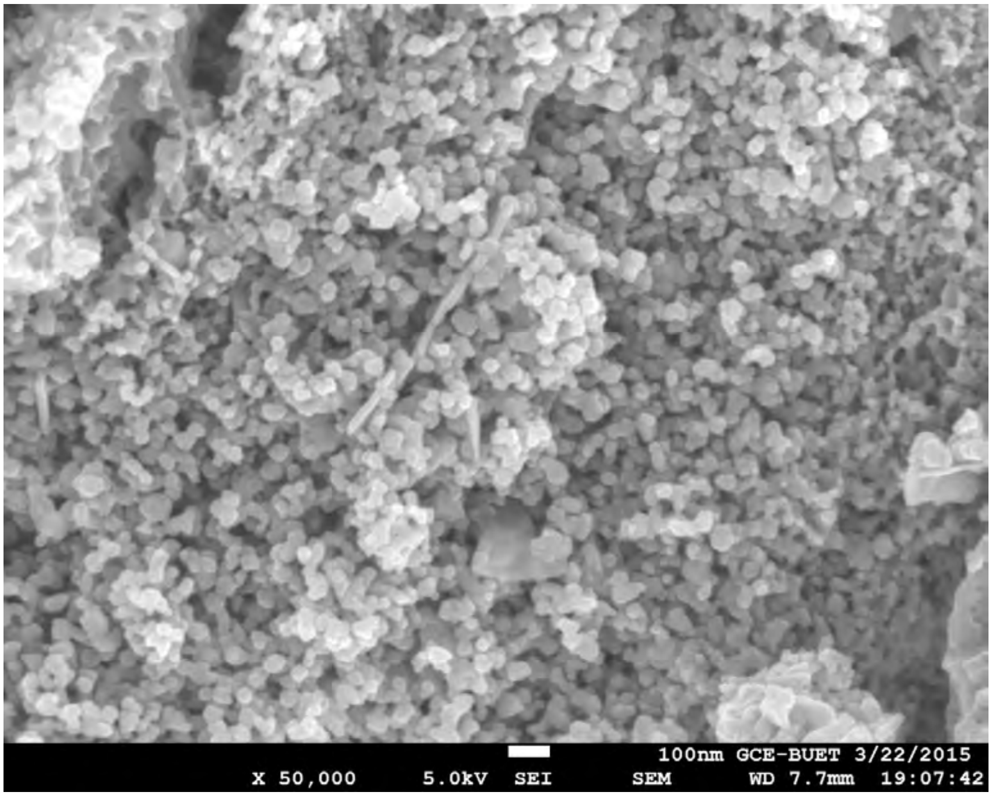

Figure 4.5: FESEM micrograph of $BiFeO_3$ powders annealed at 400^oC for 2 hour (Test 4).

For test condition 4, the concentration of ethylene glycol was 0.05. The FESEM micrograph (Figure 4.5) of the synthesized powder at this condition clearly demonstrated the formation of very fine homogenous and nearly spherical nanoparticles with very little agglomeration effect. And hence we inferred the test 4 as optimum condition to synthesize $BiFeO_3$ nanoparticles with desired size and shape. Further synthesis to characterize the material was carried out with the same test conditions.

4.3 Thermogravimetric (TG) analysis :

TG analysis was performed to investigate the thermal decomposition behavior of precursor xerogel.

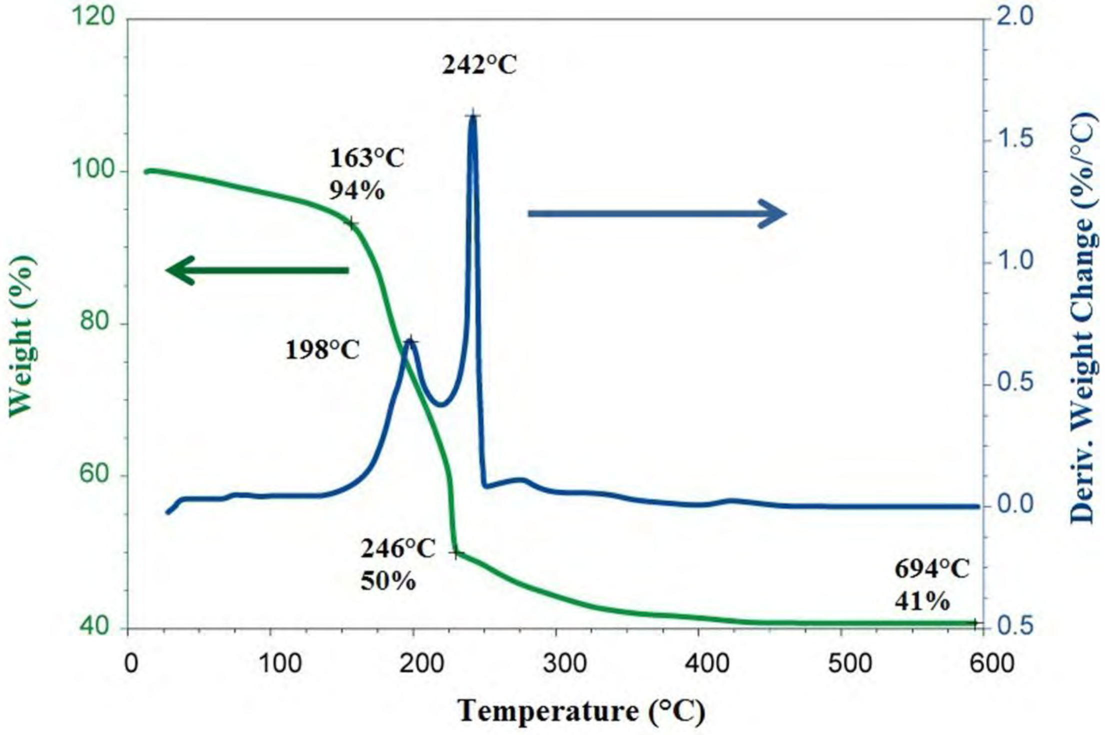

Figure 4.6: Thermogravimetric analysis curve of $BiFeO_3$ precursor xerogel.

Figure 4.6 shows thermogravimetric analysis curve of the $BiFeO_3$ precursor xerogel. The initial uniform weight loss (6%) up to 163°C is assumed to occur due to the dehydration of precursor xerogel. It is also evident that the major weight loss (44%) is accompanied with the appearance of two peaks in the derivative weight change curve. The first peak occurring at 198°C can be ascribed to the decomposition of NO_3^-, uncomplexed COO–groups of citric acid and some side-chain groups like O–H and C–H. The presence of these groups in precursor xerogel is confirmed from the FTIR spectroscopy as shown in Figure 4.7. The second peak at 242°C associated with maximum weight loss can be attributed to the decomposition of complexed polymer backbone and combustions of most of the organic materials [61, 62]. No further peak is detected above 300°C which indicates that the decomposition of nitrates and other organic phases is almost completed. The advantage of using citric acid instead of other complexing agent is that it facilitates the attainment of $BiFeO_3$ phase at much lower temperature because of its relatively low decomposition temperature (150°C) [63]. The continuous weight loss observed in Figure 4.6 between 300-500°C can be described as the removal of trapped gases from porous xerogel [61].

4.4 Fourier transform infrared spectroscopy:

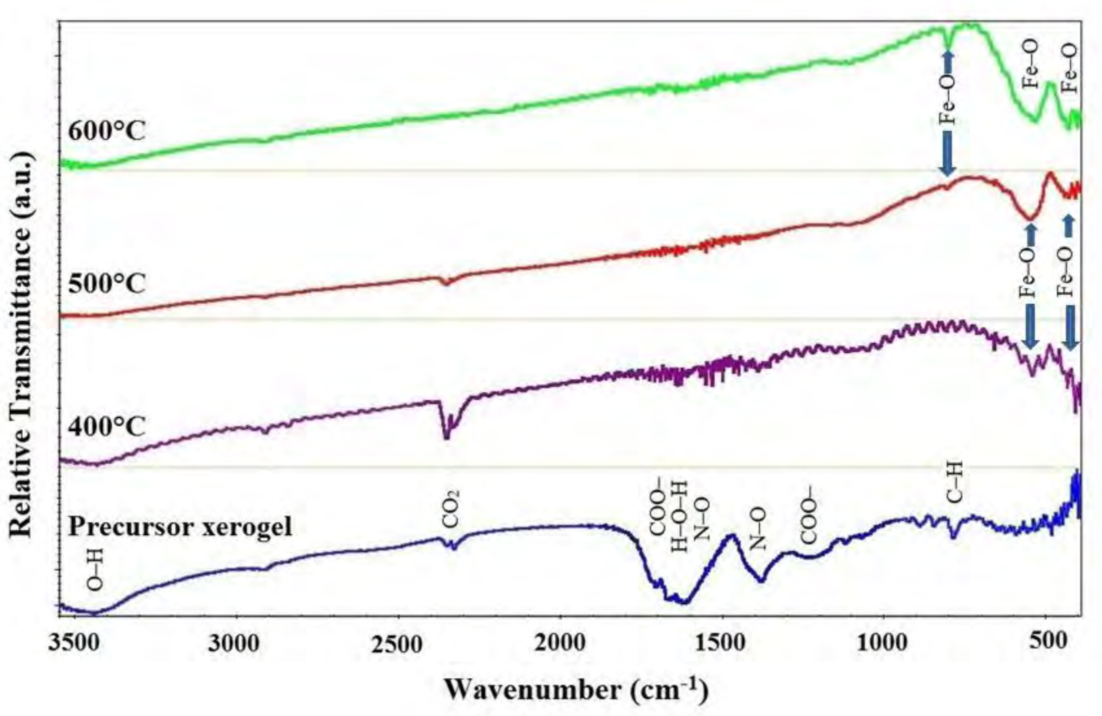

Figure 4.7: FTIR spectra of the $BiFeO_3$ precursor xerogel before and after annealing at different temperatures.

Figure 4.7 presents the FTIR spectra of the precursor xerogel before and after annealing at different temperatures. For the $BiFeO_3$ precursor, the broad absorption band in the range of 3,453 cm^{-1} can be attributed to strong O–H stretching originated from ethylene glycol or condensed products [61, 62]. Moreover, the absorption band at 1,713 and 1,248 cm^{-1} respectively can be assigned to strong C=O and C–O stretching of the COO– group of acetate ligands. It can also be seen that the strong H–O–H bending vibration of water molecule in the precursor is prominent at around 1,634 cm^{-1} in the spectra. The strong asymmetric and medium symmetric stretching vibration bonds of N–O from nitro compounds are also reported at 1,558 and 1,386 cm^{-1} respectively. In addition the medium absorption band located at around 795 cm^{-1} indicates the existence of C–H bond [64, 65]. It can also be noticed that all these precursor intensities are suppressed after annealing at 400°C. Furthermore, the sharp absorption doublet for annealed samples noticed at around 2350cm^{-1} can be attributed to the ambient carbon dioxide suggesting the decomposition of carbonaceous backbone. The amount of CO_2 decreases with annealing temperature which is the cause of continuous weight loss above 250°C as depicted in Figure 4.6 which was discussed earlier in section 4.3. Our results are concomitant with some previous published results [61, 64].

The FTIR spectra of the annealed sample at 400°C shows two absorption peaks at 542 and 438 cm^{-1} which are attributed to the Fe–O stretching and bending vibrations respectively. These are the characteristics of octahedral FeO_6 groups in the perovskite compounds and demonstrate the formation of $BiFeO_3$ phase [66]. With further increase of the annealing temperature the two Fe–O vibration peaks become prominent with the appearance of another Fe–O peak at 812 cm^{-1} which matures considerably above 500°C, implying the attainment of highly crystalline $BiFeO_3$ phase [67, 68].

4.5 Phase study:

XRD patterns of particles annealed at different temperatures before and after washing with CH_3COOH are shown, respectively, in Figure 4.8(a) and (b). To promote the formation of $BiFeO_3$, the samples were heat treated at temperatures ranging from 400 to 600°C for 2 hrs. Usually a strong acid (HNO_3) is used to remove the secondary phases that are formed during synthesis of $BiFeO_3$ nanoparticles. But HNO_3 may dissolve the $BiFeO_3$ phase [38]. So CH_3COOH, a week acid was used for washing purpose in this research.

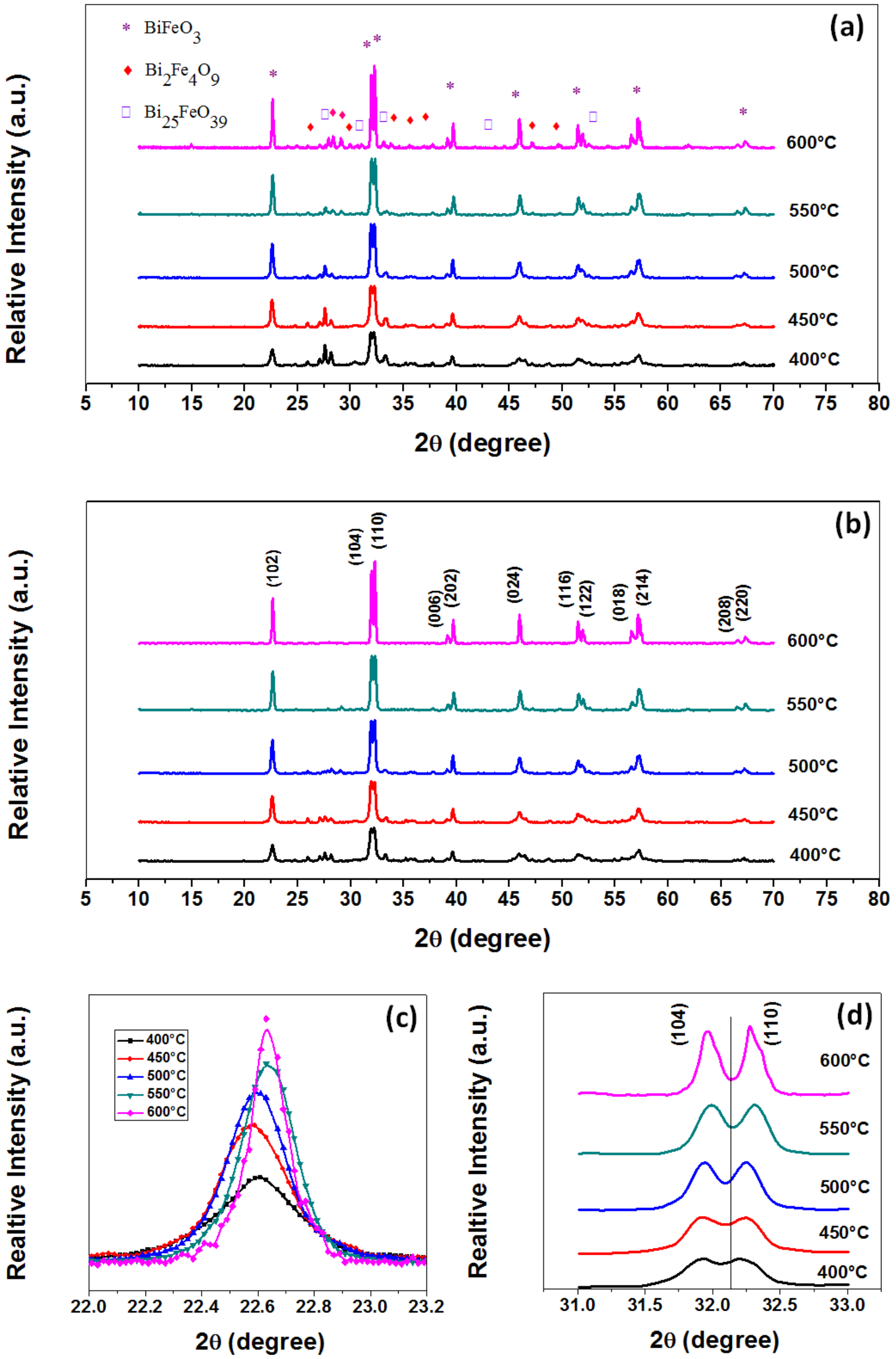

Figure 4.8: X-ray diffraction patterns of $BiFeO_3$ particles annealed at different temperatures (a) before washing, (b) after washing with acetic acid. (c) Magnified XRD patterns of (102) reflection plane and (d) magnified XRD patterns of (104) and (110) reflection plane for washed samples.

Generally, Bi_2O_3 and mullite $Bi_2Fe_4O_9$ are frequently reported secondary phases that are formed during synthesis of $BiFeO_3$. The Bi_2O_3 secondary phase is actually sillenite ($Bi_{25}FeO_{39}$) that is isostructural to γ-Bi_2O_3. Researchers have proposed different reasons for the appearance of these phases. The low temperature stability of impurity phases, metastable and off-stoichiometric nature of $BiFeO_3$ are thought to be the prime causes for the formation of secondary phases [69-71]. However, removal of these phases is important from the application point of view because they increase leakage current and deteriorate ferroelectric property [72]. It can be noticed from XRD pattern in Figure 4.8(a) that with increasing temperature all the fundamental peaks related to $BiFeO_3$ phase become stronger while that of secondary phases weaken. Further washing of the annealed samples demonstrates noticeable effect to eliminate both the secondary phases as shown in Figure 4.8(b).

The average crystallite size (*d*) was calculated from the XRD patterns using the Scherrer formula, $d = k\lambda/\beta\cos\theta$, where k is the dimensionless shape factor with a typical value of about 0.9, λ is the wavelength of Cu Kα radiation with the value of 1.5418 Å, θ is the Bragg angle for the (102) diffraction peak and β is the full width at half maximum (FWHM) intensity of the corresponding diffraction peak. The enlarged (102) diffraction peak as demonstrated in Figure 4.8 (c) clearly shows decreasing of the FWHM due to increasing particle size with annealing temperature. The calculated particle sizes are tabulated in table 4.2. From Figure 4.8(d), it is noticeable that decrease in splitting and shifting of (104) and (110) peaks around $2\theta=32°$ indicate decrease of rhombohedral symmetry and increase of orthorhombic symmetry [12].

Table 4.2: Particle size and magnetic parameters of $BiFeO_3$ samples annealed at different temperatures

Annealing Temperature (°C)	**Particle size (nm)**	**Saturation magnetization (emu/g)**	**Coercivity, 2Hc (Oe)**
400	**21**	**7.5**	**83**
450	**31**	**5.9**	**100.8**
500	**35**	**4.0**	**138.2**
550	**40**	**1.4**	**199.4**
600	**68**	**0.3**	**268.7**
800	**822**	**0.1**	**-**

4.6 FESEM micrograph analysis:

Figure 4.9 shows the FESEM micrographs of $BiFeO_3$ powders annealed at temperature range 400-800°C for 2 hrs. With increasing annealing temperature particle size increases. Reduction of the total surface area by an increase in the average size of the particles is the driving force behind coarsening.

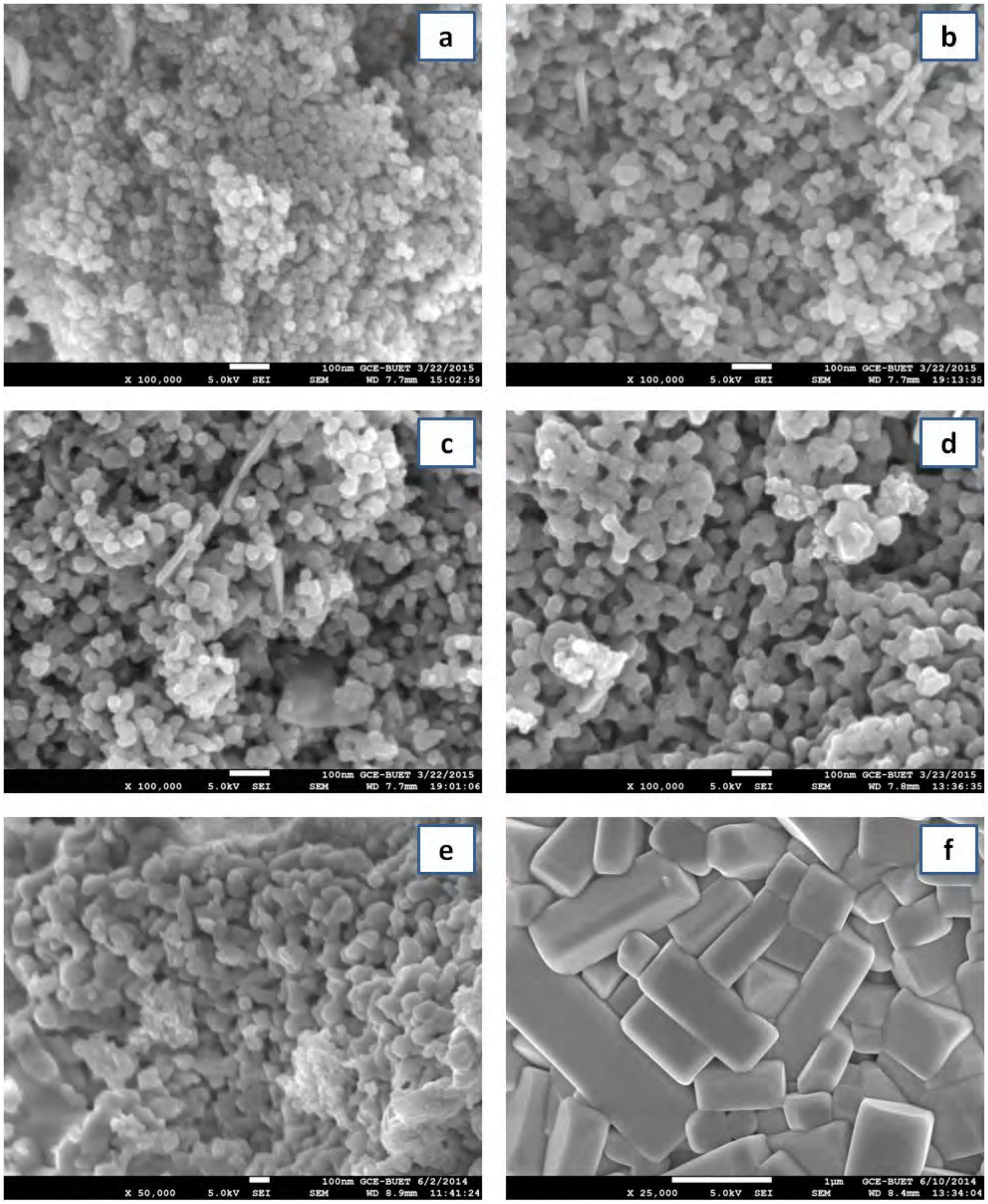

Figure 4.9: FESEM micrograph of $BiFeO_3$ powders annealed at (a) 400°C, (b) 450°C, (c) 500°C, (d) 550°C, (e) 600°C and (f) 800°C for 2 hrs in air.

There are several mechanisms like evaporation-condensation, surface diffusion and lattice diffusion from the surface to the neck area which can lead to coarsening. Another mechanism known as Ostwald ripening can be active during coarsening. At high temperature vapor pressure is high on smaller particles than coarser particles. So small particles vaporize and condense on larger particles. In this mechanism attainment of uniform particle size distribution is difficult.

It is evident from the figure that the particle sizes observed from FESEM micrograph are quite compatible with that of XRD results. This suggests that the nanoparticles are single crystalline [65]. The observed nanoparticles are nearly spherical in shape with uniform size distribution when annealed up to 600°C. But for the $BiFeO_3$ sample annealed at 800°C showed stable cubic morphology which differs from that of samples annealed at lower temperatures [73].

4.7 Magnetic property analysis

The magnetization vs. applied field (M-H) measurements of the $BiFeO_3$ powders was carried out at different temperatures in order to investigate the magnetic behavior. The room temperature magnetic hysteresis loops of $BiFeO_3$ powders annealed at 400°C, 450°C, 500°C, 550°C, 600°C and 800°C are shown in Figure 4.10(a). Expanded M–H loops are presented in Figure 4.10 (b) with inset showing dependence of coercivity on particle size. Strong size dependent magnetic parameters are vivid in these figures. The magnetic parameters associated with $BiFeO_3$ particle size are summarized in Table 4.2. The linear M–H relationship observed in Figure 4.10 (a), for the bulk $BiFeO_3$ powder annealed at 800°C suggests antiferromagnetic ordering with magnetization value as low as 0.1 emu/g. Low magnetization is attributed to the spiral spin structure in bulk $BiFeO_3$. The incommensurate spin cycloid with wave length of 62 nm which continues through the crystal suppressing macroscopic magnetization [37].

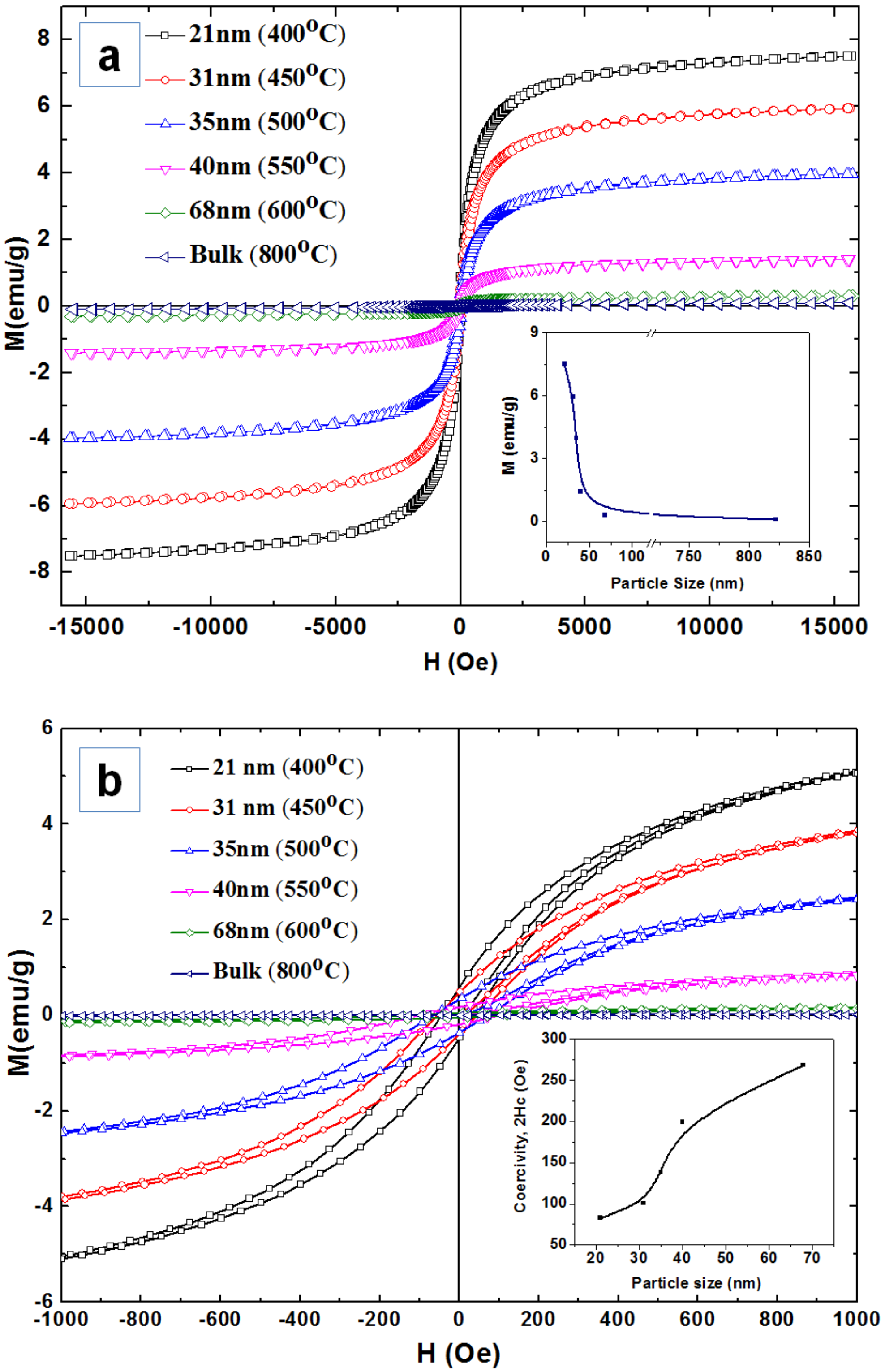

Figure 4.10: (a) M–H hysteresis loops for $BiFeO_3$ powders with indicated sizes at 300 K. The inset shows change of magnetization values at 16.5 kOe as a function of particle size. (b) Expanded plots of magnetization up to applied field of 500 Oe with inset showing dependence of coercivity on particle size.

However, synthesized nanoparticles with size close to or less than 62 nm showed a significant ferromagnetic order at room temperature and a strong size dependent values of magnetization and coercivity are observed. Magnetization values of 1.4 to 7.5 emu/g are reported in the present study for the particle size ranging between 21 and 40 nm. A dramatic increase in magnetization of two orders of magnitude is observed for the nanosized sample compared with that of bulk $BiFeO_3$. The apparent ferromagnetism for nanosized $BiFeO_3$ can be attributed to the destruction of the spiral modulated antiferromagnetic long range order [35]. A summary of saturation magnetization values as a function of particle size is also plotted in the inset of Figure 4.10 (a). It is obvious that the magnetic properties of $BiFeO_3$ powders with critical dimension below 62 nm strongly depend on size of the nanoparticles. Though bulk $BiFeO_3$ is antiferromagnetic, almost a linear increase of magnetization with decreasing particle size can be modeled as antiferromagnetic core and ferromagnetic surface [37]. Essentially the long range antiferromagnetic spiral spin structure is frequently disturbed at the particle surface due to the disruption of Fe-O bond. The missing oxygen ions are thought to be the origin of surface spin disorder by virtue of uncompensated spins from Fe^{3+} ions [74]. With decreasing particle size the surface spin disorder becomes remarkable due to the large surface to volume ratio. This uncompensated spins at the surface can contribute significantly to the particle‟s overall magnetization. Another source of ferromagnetic ordering in $BiFeO_3$ nanostructures may be assigned to the lattice distortion associated with decreasing particle size leading to the suppression of spiral spin order [12]. The rhombohedral to orthorhombic distortion can change the (180°- φ) Fe-O-Fe angle. The strong ferromagnetic ordering in this study can be correlated with the Fe-O-Fe distortion which is the basis of Goodenough-Kanamori rule [75-77].

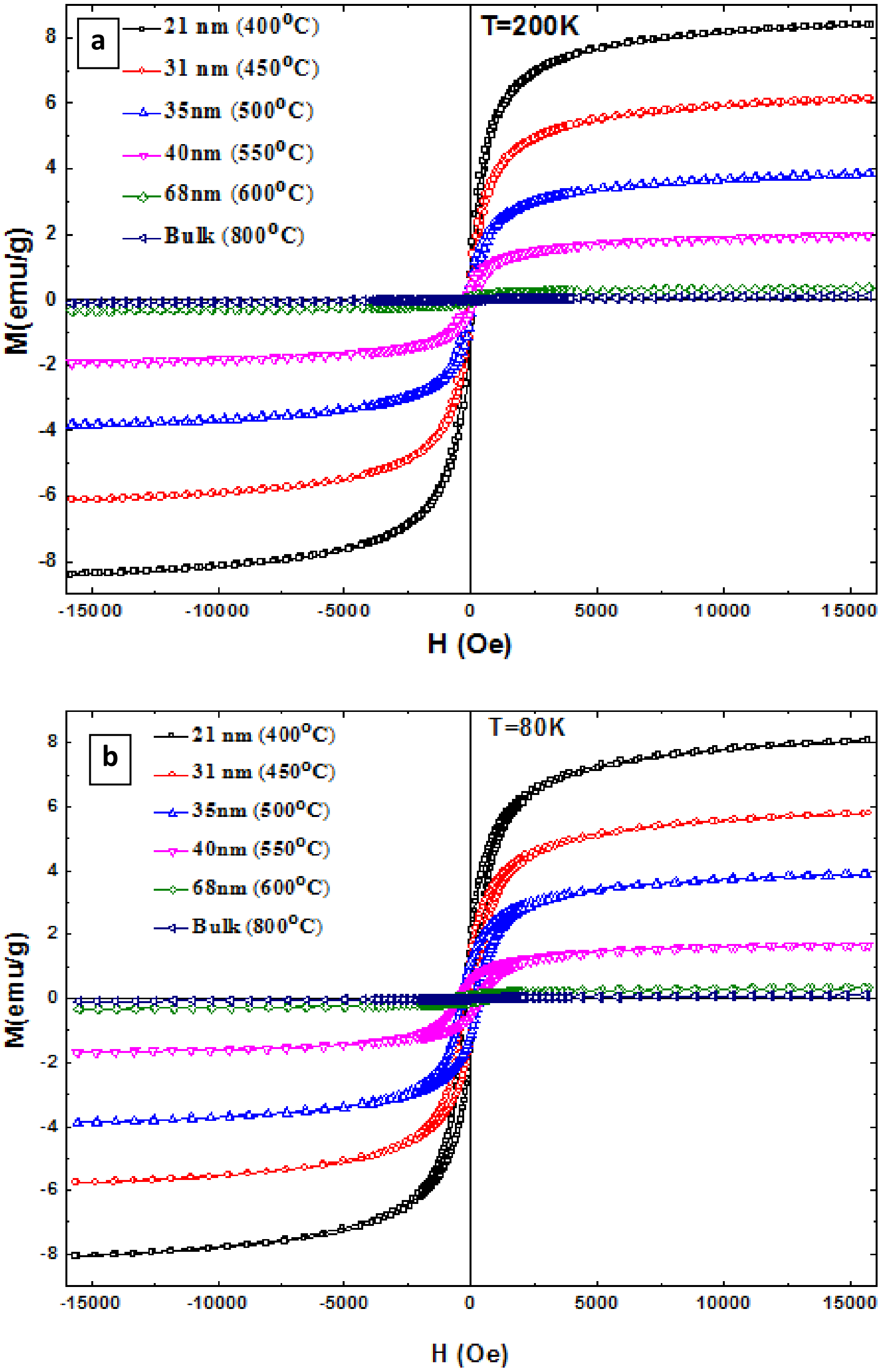

Figure 4.11: M–H hysteresis loops for $BiFeO_3$ powders with indicated sizes at (a) 200 K and (b)80K

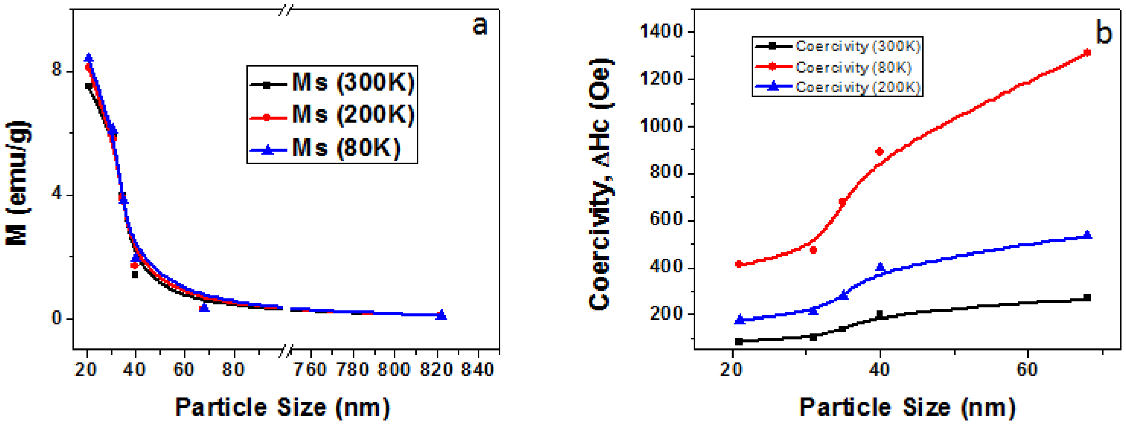

Figure 4.12: Dependence of (a) magnetization and (b) coercivity on particle size of synthesized $BiFeO_3$ powders.

Magnetic hysteresis loops for $BiFeO_3$ powders at measurement temperature 200K and 80K are shown in Figure 4.11 (a) and (b) respectively. The M-H behavior at lower temperatures of the synthesized powders is found to be similar with that at room temperature. Bulk $BiFeO_3$ is antiferromagnetic whereas nanoparticles with size in the order of smaller than 62 nm are ferromagnetic. However, magnetization and coercivity values increase somewhat with decreasing measuring temperature. The particle size dependent magnetism and coercivity are shown in Figure 4.12 (a) and (b) respectively. Though magnetization increases slightly, coercivity increases significantly with decreasing measurement temperature because anisotropy is temperature dependent phenomena. With decreasing temperature both the magnetocrystalline and magnetostriction anisotropy energy increases with resultant increase of coercivity.

Moreover, though the particle size dependent magnetic properties with a critical size scale of 62 nm is in good agreement with some previous studies, the synthesized $BiFeO_3$ nanoparticles in this study show somewhat higher saturation magnetization and nearly saturated hysteresis loops at lower applied field [35-37]. The earlier report anticipated that improvement in ferromagnetism could be achieved by tailoring shape anisotropy of the synthesized powders [35]. With decreasing particle size shape anisotropy becomes dominant over magnetocrystalline anisotropy. For an object the applied magnetic field is somewhat masked by a component known as demagnetization field due to the shape anisotropy. The internal magnetic field, H for an applied uniform magnetic field, H_0 can be represented by the following equation,

$$H = H_0 - NM_0$$

where M_0 is the magnetization value and N is the demagnetization factor. For homogenously distributed spherical particles the value of demagnetization factor is smaller than that of irregular shape. Furthermore, the decrease of coercivity with decreasing particle size as shown in the inset of Figure 4.10 (b), clearly demonstrates the transition of synthesized $BiFeO_3$ powders from single domain size towards superparamagnetic region resulting in reduced values of anisotropy energy. The increased ferromagnetism with decreasing particle size may be interpreted by the reduced anisotropy energy and lower demagnetization factor of the synthesized spherical particles. However, sometimes the magnetic properties of $BiFeO_3$ may be overshadowed by the presence of some Fe_3O_4 impurity phase, the FTIR and XRD analysis discard any evidence for the presence of such phase in the synthesized powders. Although minor impurity phases ($Bi_{25}FeO_{39}$, $Bi_2Fe_4O_9$) are present, they do very little or no contribution to the observed ferromagnetic properties of the $BiFeO_3$ samples [75, 78].

5. CONCLUSION

The objective of this thesis project was to develop a novel multiferroic material exhibiting improved ferromagnetic properties by controlling particle size of $BiFeO_3$ nanostructures. This goal was successfully achieved. Although $BiFeO_3$ is considered a promising candidate for applications in magnetic storage devices, its weak ferromagnetic property is a major problem limiting its practical applications. The magnetization values of the synthesized nanoparticles were found to increase significantly with decreasing particle size. Magnetization value of as high as 7.5 emu/g was reported for the sample with particle size of 21 nm. This greatly improved ferromagnetic ordering may find some important applications since the antiferromagnetic nature is the primary weakness of $BiFeO_3$ multiferroics. The salient features of the present study may be summarized as follows:

I. $BiFeO_3$ nanoparticles were synthesized via a soft chemical route. Nearly pure and well crystallized $BiFeO_3$ powders were obtained by washing with acetic acid instead of conventional nitric acid.

II. TG and FTIR analysis revealed that $BiFeO_3$ nanoparticles were obtained at relatively low temperature.

III. Ethylene glycol with an optimun concentration of 0.05 M was successfully used as surfactant agent during synthesis to obtain a homogenous and uniform particle size distribution.

IV. The sizes of the synthesized $BiFeO_3$ nanostructures annealed at 400, 450, 500, 550and 600^0C were noted to be 21 nm, 31 nm, 35 nm, 40 nm and 68 nm respectively.

V. Magnetic hysteresis loop measurement showed substantial improvement of saturation magnetization with reported values of 7.5 emu/g, 5.9 emu/g, 4.0 emu/g and 1.4 emu/g for 21 nm, 31 nm, 35 nm and 40 nm size powder samples respectively, whereas bulk $BiFeO_3$ is antiferromagnetic.

VI. Size confinement effect, surface spin disorder, distorted spin cycloid, lower anisotropy and single domain nature of the synthesized particles are considered as possible reasons for the improved ferromagnetic properties.

6. SUGGESTIONS FOR FUTURE WORK

- Synthesis of $BiFeO_3$ nanoparticles using different chelating agent and surfactant.
- Synthesis of doped (Ba, Mn, La, Gd, Nd, Nb, Dy etc) $BiFeO_3$ nanoparticles .
- Fabrication of thin film to reproduce high magnetization in this structure.
- Commercialization of the synthesis technique.
- Fabricating memory devices using the developed material on availability of the device fabrication lab equipments.

References:

---

1. W. Eerenstein, N. D. Mathur, J. F. Scott, „Multiferroic and magnetoelectric materials‟ Nature, Vol. 442, 2006, pp 759-765.
2. Nicola A. Hill „Why are there so few magnetic ferroelectrics?‟ Journal of Physical Chemistry B, Vol. 104, 2000, pp 6694-6709.
3. Gustau Catalan, James F. Scott „Physics and applications of bismuth ferrite‟ Advanced Materials, Vol. 21, 2009, pp 2463-2485.
4. S.Kazhugasalamoorthy, P. Jegatheesan, R. Mohandoss, N. V. Giridharan, B. Karthikeyan, R. J.Joseyphus, S. Dhanuskodi „Investigations on the properties of pure and rare earth modified bismuth ferrite ceramics‟ Journal of Alloys and Compounds, Vol. 493, 2010, pp 569-572.
5. Izabela Sosnowska, Masaki Azuma, Radosław Przeniosło, Dariusz Wardecki, Wei-tin Chen, Kengo Oka, Yuichi Shimakawa „Crystal and magnetic structure in Co-substituted BiFeO$_3$‟ Inorganic Chemistry, Vol. 52, 2013, 13269-13277.
6. F. Kubel, H. Schmid „Structure of a ferroelectric and ferroelastic monodomain crystal of the perovskite BiFeO$_3$‟ Acta Crystallographica B, Vol. 46, 1990, pp 698-702.
7. A. Palewicz, I. Sosnowska, R. Przeniosło, A.W. Hewat „BiFeO$_3$ crystal structure at low temperatures‟ Acta Physica Polonica, Vol. A 117, 2010, pp 296-301.
8. Yingbang Yao, Wenchao Liu, Yukkwan Chan, Chiwah Leung, Cheeleung Mak „Studies of Rare-Earth-Doped BiFeO$_3$ Ceramics‟ Journal of Applied Ceramic Technology, Vol. 8, 2011, pp 1246-1253.
9. A. Mukherjee, S. Basu , P.K. Manna, S.M. Yusuf, M. Pal „Enhancement of multiferroic properties of nanocrystalline BiFeO$_3$ powder by Gd-doping‟ Journal of Alloys and Compounds, Vol. 598, 2014, pp 142-150.
10. Tae-Jin Park, C. Georgia Papaefthymiou, J. Arthur Viescas, R. Arnold Moodenbaugh, S. Stanislaus Wong „Size-dependent magnetic properties of single-crystalline multiferroic BiFeO$_3$ nanoparticles‟ Nano Letters, Vol. 7 , 2007, pp 766-772.
11. Fengzhen Huang, Zhijun Wang, Xiaomei Lu, Junting Zhang, Kangli Min, Weiwei Lin, Ruixia Ti, TingTing Xu, Ju He, Chen Yue, Jinsong Zhu „Peculiar magnetism of BiFeO$_3$

nanoparticles with size approaching the period of the spiral spin structure‟ Scientific Reports, Vol. 3, 2013, pp 2907.

12. Gurmeet Singh Lotey, N. K. Verma „Structural, magnetic, and electrical properties of Gd-doped $BiFeO_3$ nanoparticles with reduced particle size‟ Journal of Nanoparticle Research, Vol. 14, 2012, pp 742.
13. J. Silva, A. Reyes, H. Esparza, H. Camacho, L. Fuentes „$BiFeO_3$: A review on synthesis, doping and crystal structure‟ Integrated Ferroelectrics, Vol. 126, 2011, pp 47-59.
14. H. Ibach, H. Luth, „Solid-State Physics: An Introduction to Principles of Materials Science‟ 4th edition, Springer Dordrecht Heildberg London New York, 2009.
15. S. Somiya, F. Aldinger, „Handbook of Advanced Ceramics: Processing and their applications‟, Vol-2, Elsevier Academic Press, 2009.
16. Singh, S. K., Ishiwara, H., Maruyama „Room temperature ferroelectric properties of Mn-substituted $BiFeO_3$ thin films deposited on Pt electrodes using chemical solution deposition‟ Applied Physics Letters, Vol. 88, 2006, pp 262908.
17. J.F. Scott, “Multiferroic Memories,” Nature materials, Vol. 6, 2007, pp 256-257.
18. M. Bibes and A. Barthelemy, “Multiferroics: Towards a magnetoelectric memory,” Nature materials, Vol. 7, 2008, pp 425-426.
19. Lane W. Martin, Ying-Hao Chu, Qian Zhan, R. Ramesh „Room temperature exchange bias and spin valves based on BiFeO3 /SrRuO3 /SrTiO3/Si (001) heterostructures‟ Applied Physics Letters Vol. 91, 2007, pp 172513.
20. J. Wang, N. A. Spaldin, R.Ramesh, „Epitaxial $BiFeO_3$ Multiferroic Thin Film Heterostructures‟ J. Science, Vol. 299, 2003, pp 1719.
21. D. Lebeugle, D. Colson, A. Forget, M. Viret, P. Bonville „Room-temperature coexistence of large electric polarization and magnetic order in $BiFeO_3$ single crystals‟ Physical Review B, Vol. 76, 2007, pp 024116.
22. Silvia Picozzi, Claude Ederer „First principles studies of multiferroic materials‟ Journal Physics: Condensed Matter Vol. 21, 2009, 303201.
23. Axel Lubk, S. Gemming, N. A. Spaldin „First-principles study of ferroelectric domain walls in multiferroic bismuth ferrite‟ Physical Review B Vol. 80, 2009, pp 104110.

24. Palkar V R, John J and Pinto R „Observation of saturated polarization and dielectric anomaly in magnetoelectric $BiFeO_3$ thin films‟ Applied Physical Letter Vol.80, 2002, pp 1628.
25. Yun K Y, Noda M, Okuyama M, Saeki H, Tabata H, Saito K „Structural and multiferroic properties of $BiFeO_3$ thin films at room temperature‟ Journal Applied Physics Vol. **96**, 2004, pp 3399.
26. S. Y. Yang „Metalorganic chemical vapor deposition of lead-free ferroelectric $BiFeO_3$ films for memory applications‟ Applied Physics Letter Vol.87, 2005, pp 102903.
27. S. Shanthy „Multiferroic $BiFeO_3$ films: candidate for room temperature micro biosensor‟ Integrated Ferroelectronics, Vol. 99, 2008, pp 77 - 85.
28. Burda, C.Chen, X. Narayanan, R. El-Sayed „Chemistry and properties of nanocrystals of different shapes.‟ Chemical Review Vol.105, 2005, pp 1025.
29. B. Gilbert, F. Huang, H. Zhang, G. A. Waychunas, J.F. Banfield. „Nanoparticles: Strained and Stiff.‟ Science, Vol. 305,2004, pp 651-654.
30. M. Yasin Shami, M.S. Awan, M. Anis-ur-Rehman „Phase pure synthesis of $BiFeO_3$ nanopowders using diverse precursor via co-precipitation method‟ Journal of Alloys and Compounds, Vol.509, 2011, pp 10139–10144.
31. Yonggang Wang, Gang Xu, Linlin Yang, Zhaohui Ren, Xiao Wei, Wenjian Weng, Piyi Du, Ge Shen, Gaorong Han „Enhanced ferromagnetic properties of multiferroic $BiCo_xFe_{1-x}O_3$ synthesized by hydrothermal method‟ Materials Letters, Vol. 62, 2008, pp 3806-3808.
32. Yuning Huo, Yi Jin, Ya Zhang „Citric acid assisted solvothermal synthesis of $BiFeO_3$microspheres with high visible-light photocatalytic activity‟ Journal of Molecular Catalysis A: Chemical, Vol. 331, 2010, pp 15–20.
33. Dimple P. Dutta, Balaji P. Mandal, Ratna Naik, Gavin Lawes, Avesh K. Tyagi ‘Magnetic, Ferroelectric, and Magnetocapacitive Properties of Sonochemically Synthesized Sc-Doped $BiFeO_3$ Nanoparticles‟ Journal of Physical Chemistry C, Vol. 117, 2013, pp 2382–2389.
34. Ting Liu, Yebin Xuw, Jingyuan Zhao “Low-temperature synthesis of $BiFeO_3$ via PVA sol–gel route” Journal of American Ceramic Society, Vol. 93, 2010, pp3637-3641.

35. Tae-Jin Park, C. Georgia Papaefthymiou, J. Arthur Viescas, R. Arnold Moodenbaugh, S. Stanislaus Wong „Size-dependent magnetic properties of single-crystalline multiferroic $BiFeO_3$ nanoparticles‟ Nano Letters Vol. 7, 2007, pp 766-772.
36. Jie Wei, Desheng Xue „Low-temperature synthesis of $BiFeO_3$ nanoparticles by ethylenediaminetetraacetic acid complexing sol–gel process‟ Materials Research Bulletin, Vol. 43 , 2008, pp 3368–3373.
37. Fengzhen Huang, Zhijun Wang, Xiaomei Lu, Junting Zhang, Kangli Min, Weiwei Lin, Ruixia Ti, TingTing Xu, Ju He, Chen Yue, Jinsong Zhu „Peculiar magnetism of $BiFeO_3$ nanoparticles with size approaching the period of the spiral spin structure‟ Scientific Reports, Vol.3 , 2013, pp 2907.
38. José Luis Ortiz-Quiñonez, David Díaz, Inti Zumeta-Dubé, Humberto Arriola-Santamaría, Israel Betancourt, Patricia Santiago-Jacinto, Noel Nava-Etzana „Easy synthesis of high-purity $BiFeO_3$ nanoparticles: new insights derived from the structural, optical, and magnetic characterization‟ Inorganic Chemistry, Vol. 52, 2013, pp10306-10317.
39. J. C. Maxwell „A Dynamical Theory of the Electromagnetic Field‟ Philosophical Transactions Royal Society London, Vol. 155, 1865, 459–512.
40. F. Duan and J. Guojun, “Introduction to Condensed Matter Physics.” World Scientific (Vol. 1), Singapore, 2005.
41. C. Kittel, “Introduction to solid state physics.” American Journal of Physics, Vol. 35, 1967, pp. 547-548.
42. E. K. H Salje, “Phase Transitions in Ferroelastic and Co-elastic Crystals.” Cambridge University Press, 1990.
43. V. Muller, A. Fuith, J. Fousek, H. Warhanek and H. Beige, “Spontaneous strain in ferroelastic incommensurate [N(CH3)4]2CuCl4 crystals,” Solid State Communications, Vol. 104, 1997, pp. 455-458.
44. L. Jian and C. M. Wayman, “Compressive behavior and domain-related shape memory effect in LaNbO4 ceramics,” Materials Letters, Vol. 26, 1996, pp 1-7.
45. R. E. Newnham, “Molecular mechanisms in smart materials,” MRS Bulletin, Vol. 22, 1997, pp. 20-34.

46. W. Cheong, M. Mostovoy, “Multiferroics: a magnetic twist for ferroelectricity, ”Nature Materials, Vol. 6, 2007, pp 13-20.
47. H.Béa, M.Gajek, M.Bibes and A.Barthélémy, „Spintronics with multiferroics‟ Journal Physics: Condensed Matter, Vol. 20, 2008, pp 434221.
48. Nicola A. Hill „Why are there so few magnetic ferroelectrics?‟ Journal of Physical Chemistry B, Vol. 104, 2000, pp 6694-6709.
49. G A Smolenskii, I E Chupis, „Ferroelectromagnets‟ Soviet Physics Uspekhi, Vol. 25, 1982, pp 475-493.
50. D.I.Khomskii, “Magnetism and ferroelectricity: why do they so seldom coexist?” Bulletin of American Physical Society C, Vol. 1, 2001, pp. 21002.
51. M. Fieberg, “Revival of the magnetoelectric effect”, Journal of Physics D: Applied Physics, Vol. 38, 2005, pp. 123.
52. A.K. Ghosh , G.D. Dwivedi, B. Chatterjee, B. Rana, A. Barmanb, S. Chatterjee, H.D. Yang, “Role of codoping on multiferroic properties at room temperature in BiFeO3 ceramic”, Solid State Communications, Vol. 166, 2013, pp 22–26.
53. T. Kimura, „Magnetic control of ferroelectric polarization‟ Nature, Vol. 426, 2003, pp 55.
54. N. Hur, S. Park „Electric polarization reversal and memory in a multiferroic material induced by magnetic fields‟ Nature, Vol. 429,2004, pp 392.
55. T. Arima „Ferroelectricity Induced by Proper-Screw Type Magnetic Order‟Journal of Physical Society of Japan, Vol. 76, 2007, pp 073702.
56. Y. J. Choi, H. T. Yi, S. Lee, Q. Huang, V. Kiryukhin, Physical Review Letter, Vol.100, 2008, 047601.
57. Nicola A. Spaldin, Sang-Wook Cheong, Ramamoorthy Ramesh „Multiferroics: past, present and future‟ Physics Today, Vol. 63, 2010, pp 38-43.
58. Smolensky G A, Isupov V A, Agronovskaya A I. „A new group of ferroelectrics-(with layered structure)‟, Journal of Sov Phys Solid State, Vol. 1, 1959, pp 149–150.
59. G. D. Achenbach, W. J. JameS, R. Gerson „Preparation of Single-Phase Polycrystalline $BiFeO_3$‟ Journal of the American Ceramic Society, Vol. **50**, 1967, pp 437
60. J. Lu, L. J. Qiao, P. Z. Fu, Y. C. Wu „Phase equilibrium of Bi_2O_3–Fe_2O_3 pseudo-binary system and growth of $BiFeO_3$ single crystal‟ Journal of Crystal Growth Vol. 318, 2011, pp 936-941.

61. Jia-Huan Xu, Hua Ke, De-Chang Jia, WenWang, Yu Zhou „Low-temperature synthesis of $BiFeO_3$ nanopowders via a sol-gel method" Journal of Alloys and Compounds, Vol. 472, 2009, pp.473-477.
62. Sushmita Ghosh, Subrata Dasgupta, Amarnath Sen, Himadri Sekhar Maiti „Low-temperature synthesis of nanosized bismuth ferrite by soft chemical route" Journal of American Ceramic Society, Vol. 88, 2005, pp. 1349-1352.
63. Samar Layek, H. C. Verma „Magnetic and Dielectric properties of multiferroic $BiFeO_3$ nanoparticles synthesized by a novel citrate combustion method" Advanced Materials Letters, Vol. 6, 2012, pp. 533-538.
64. Chyi-Ching Hwang ,Tsung-Yung Wu, Jun Wan, Jih-Sheng Tsai „Development of a novel combustion synthesis method for synthesizing of ceramic oxide powders" Materials Science and Engineering: B Vol. 111, 2004, pp. 49-56.
65. H. Yang , T. Xian , Z. Q. Wei , J. F. Dai ,J. L. Jiang, W. J. Feng „Size-controlled synthesis of $BiFeO_3$ nanoparticles by a soft-chemistry route" Journal of Sol-Gel Science and Technology, Vol. 58, 2011, pp. 238-243.
66. Ting Liu, Yebin Xuw, Jingyuan Zhao „Low-temperature synthesis of $BiFeO_3$ via PVA sol-gel route" Journal of American Ceramic Society, Vol. 93, 2010, pp. 3637-3641.
67. R. P. S. M. Lobo, R. L. Moreira, D. Lebeugle, D. Colson „Infrared phonon dynamics of a multiferroic $BiFeO_3$ single crystal" Physical Review B, Vol. 76, 2007, pp. 172105.
68. W. Kaczmarek, A. Graja „Lattice dynamics study of the solid solution $(Bi_{1-x}La_x)$ FeO_3 by i.r. spectroscopy" Solid State Communications, Vol. 17, 1975, pp. 851-853.
69. Archna Sagdeo , Puspen Mondal, Anuj Upadhyay, A.K. Sinha, A.K. Srivastava, S.M. Gupta, P. Chowdhury, Tapas Ganguli, S.K. Deb „Correlation of microstructural and physical properties in bulk $BiFeO_3$ prepared by rapid liquid-phase sintering" Solid State Sciences, Vol. 18 , 2013, pp. 1-9.
70. Matjaz Valant, Anna-Karin Axelsson, Neil Alford „Peculiarities of a solid-state synthesis of multiferroic polycrystalline $BiFeO_3$" Chemistry of Materials, Vol. 19, 2007, pp. 5431-5436.
71. J. Lu, L. J. Qiao, P. Z. Fu, Y. C. Wu „Phase equilibrium of Bi_2O_3–Fe_2O_3 pseudo-binary system and growth of $BiFeO_3$ single crystal" Journal of Crystal Growth, Vol. 318, 2011, pp. 936-941.

72. Y. P. Wang, L. Zhou, M. F. Zhang, X. Y. Chen, J.-M. Liu, Z. G. Liu „Room-temperature saturated ferroelectric polarization in $BiFeO_3$ ceramics synthesized by rapid liquid phase sintering" Applied Physics Letters, Vol. 84, 2004, pp. 1731.
73. Jian-Ping Zhou, Ruo-Lin Yang, Rui-Juan Xiao, Xiao-Ming Chen, Chao-Yong Deng „Structure and phase transition of $BiFeO_3$ cubic micro-particles prepared by hydrothermal method" Materials Research Bulletin, Vol. 47, 2012, pp. 3630-3636.
74. V. Annapu Reddy, N.P. Pathak, R. Nath „Particle size dependent magnetic properties and phase transitions in multiferroic $BiFeO_3$ nano-particles" Journal of Alloys and Compounds, Vol. 543, 2012, pp. 206-212.
75. Weiwei Hu, Yan Chen, Hongming Yuan, Guanghua Li, Yu Qiao, Yuanyuan Qin, Shouhua Feng „Structure, Magnetic, and Ferroelectric Properties of $Bi_{1-x}Gd_xFeO_3$Nanoparticles" Journal of Physical Chemistry C, Vol. 115, 2011, pp. 8869-8875.
76. John B. Goodenough „An interpretation of the magnetic properties of the perovskite-type mixed crystals $La_{1-x}Sr_xCoO_{3-\lambda}$" Journal of Physics and Chemistry of Solids, Vol. 6, 1958, pp. 287-297.
77. Junjiro Kanamori „Superexchange interaction and symmetry properties of electron orbitals" Journal of Physics and Chemistry of Solids, Vol. 10, 1959, pp. 87-98.
78. Yijun Chen, Qingsheng Wu , Jing Zhao „Selective synthesis on structures and morphologies of $Bi_xFe_yO_z$ nanomaterials with disparate magnetism through time control" Journal of Alloys and Compounds, Vol. 487, 2009, pp. 599–604.